Lab on a Chip

CRITICAL REVIEW

View Article Online
View Journal | View Issue

Cite this: *Lab Chip*, 2026, **26**, 1528

On-chip characterization of cell mechanics assisted by external physical fields and artificial intelligence

Jingjin Ge,†[a] Chenhao Bai,†[a] Zhuo Chen,*[a] Toshio Fukuda,[b] Tatsuo Arai[ac] and Xiaoming Liu *[a]

Traditional microfluidic chips for single-cell mechanical characterization face challenges such as cell aggregation and low throughput, limiting their clinical applicability. While fluid-driven methods such as constricted extrusion, pipette aspiration, and shear-induced or stretch-induced deformation have demonstrated laboratory success, they require improvements in accuracy and scalability. To overcome these limitations, integration of external physical fields, including acoustic, optical, electrical, and magnetic, enables non-contact, high-throughput cell operations and analysis. Acoustic waves and magnetic fields provide precise control over cell deformation, optical tweezers enable contact-free trapping, and electric fields facilitate dielectrophoretic manipulation. These techniques improve measurement sensitivity and throughput, making them more suitable for clinical applications, but also increase follow-up processing time. Artificial intelligence (AI) further enhances microfluidic automation across all these methodologies by enabling real-time image processing, parameter optimization, and data analysis to shorten processing time. This review particularly explores how AI is poised to solve fundamental, long-standing problems in cell mechanics that are intractable for conventional methods. Future microfluidic systems will integrate multiple physical fields controlled with AI, improving precision and scalability. The convergence of microfluidics, external fields, and AI is expected to revolutionize single-cell mechanobiology, advancing both fundamental research and clinical applications.

Received 8th September 2025,
Accepted 6th December 2025

DOI: 10.1039/d5lc00855g

rsc.li/loc

Introduction

Cellular mechanical properties, such as stiffness, elasticity, and viscoelasticity, are critical to understanding functions and behaviours of cells in biophysics, medicine, and biology.[1] These properties are governed by structural components[2] like the cell membrane,[3] cytoskeleton,[4,5] and nucleus,[5,6] and vary considerably under physiological and pathological conditions.[7] For example, in hematological disorders, the increased stiffness and reduced deformability of red blood cells (RBCs) in iron deficiency anemia not only underpin the disease pathophysiology but also present a compelling diagnostic biomarker.[8] In contrast, cancer cells often display higher elasticity during metastasis,[9] enhancing their migratory capacity.[10] Even within the same cancer type, mechanical properties such as hardness and deformability evolve during different stages of disease progression.[11] Such variations underscore the importance of accurately characterizing cellular mechanics. Beyond diagnostics, the accurate characterization of cellular mechanics holds transformative potential in drug development, where it can serve as a label-free readout for screening the efficacy of cytoskeleton-targeting chemotherapeutics.[12,13] It is these high-impact applications that demand the development of more robust, high-throughput, and automated characterization tools beyond conventional methods.[14]

Accurate characterization of cellular mechanical properties faces significant challenges due to cell complexity and dynamic nature. Atomic force microscopy (AFM) has been widely used to address these challenges,[15] which provides high-precision mechanical measurements by applying controlled forces to cells and measuring their deformation at the nanoscale.[16] However, AFM is limited by poor throughput, typically low to one cell per minute, making it unsuitable for studying rare cell populations or large datasets.[17]

Microfluidic platforms have emerged as a promising alternative, enabling high-throughput, non-invasive, and

[a] *Key Laboratory of Biomimetic Robots and Systems, Ministry of Education, State Key Laboratory of Intelligent Control and Decision of Complex System, School of Mechatronics Engineering Beijing Institute of Technology, Beijing 100081, China. E-mail: zchen97@bit.edu.cn, liuxiaoming555@bit.edu.cn*
[b] *Institute of Innovation for Future Society, Nagoya University, Nagoya, 4648601, Japan*
[c] *Center for Neuroscience and Biomedical Engineering, The University of Electro-Communications, Tokyo, 1828585, Japan*
† These authors contributed equally to this work.

quantitative single-cell analysis.[18,19] By applying controlled mechanical forces, such as shear stress, compression, or stretching, these systems allow real-time study of cellular deformation and recovery.[20] However, challenges remain in achieving high accuracy and efficiency due to the channel geometry and flow dynamics. Additionally, these systems are often constrained by requiring manual intervention and data analysis, which can be time-consuming and prone to human error.

External physical fields, including electrical, optical, magnetic, and acoustic, have been integrated into microfluidic systems to address these limitations.[21–24] These fields enable precise cell manipulation and mechanical characterization.[25] Specifically, electrical fields, such as those generated in dielectrophoresis, are utilized for dynamic fatigue characterization.[21] Optical tweezers permit non-contact trapping and mechanical probing,[26,27] whereas magnetic fields facilitate the deformation of cells labelled with nanoparticles.[23] Concurrently, acoustic fields operate by inducing shear waves to non-invasively probe cellular elasticity.[28] However, despite their versatility, these methods often face inherent challenges in achieving real-time, high-throughput, and automated analysis.[14] The characterization process typically generates complex, high-dimensional datasets that are difficult to interpret manually and can be a significant source of experimental burden and time cost.[11]

Here, the concept of automation refers to the process of achieving predetermined objectives with minimal or no direct human involvement. Artificial intelligence (AI), which provides a powerful technical assistance for automation, performs cognitive functions by learning from data to enable perception, classification, and optimization.[29,30] This is where AI offers transformative potential.

Current AI integration enhances microfluidic cell mechanical characterization by improving three core functions: (i) perception and feature extraction, (ii) data analysis and model building, (iii) decision-making and control. Perception and feature extraction are advanced through computer vision, primarily using OpenCV or convolutional neural networks (CNNs) like mask region-based CNN (MASK-RCNN) and BiSeNet to automate cell identification, tracking, and deformation quantification.[31–33] Data analysis and model building leverage machine learning techniques, including support vector machines (SVM) and random forests for mechanophenotyping classification, alongside deep neural networks (DNN) and backpropagation neural networks (BPNN) for regressing properties like stiffness and viscoelasticity from imaging and hydrodynamic data.[34–39] These approaches enable automated, high-accuracy extraction of mechanical properties, empower high-throughput analysis, and facilitate iterative optimization of experimental parameter. In research settings, decision-making and control

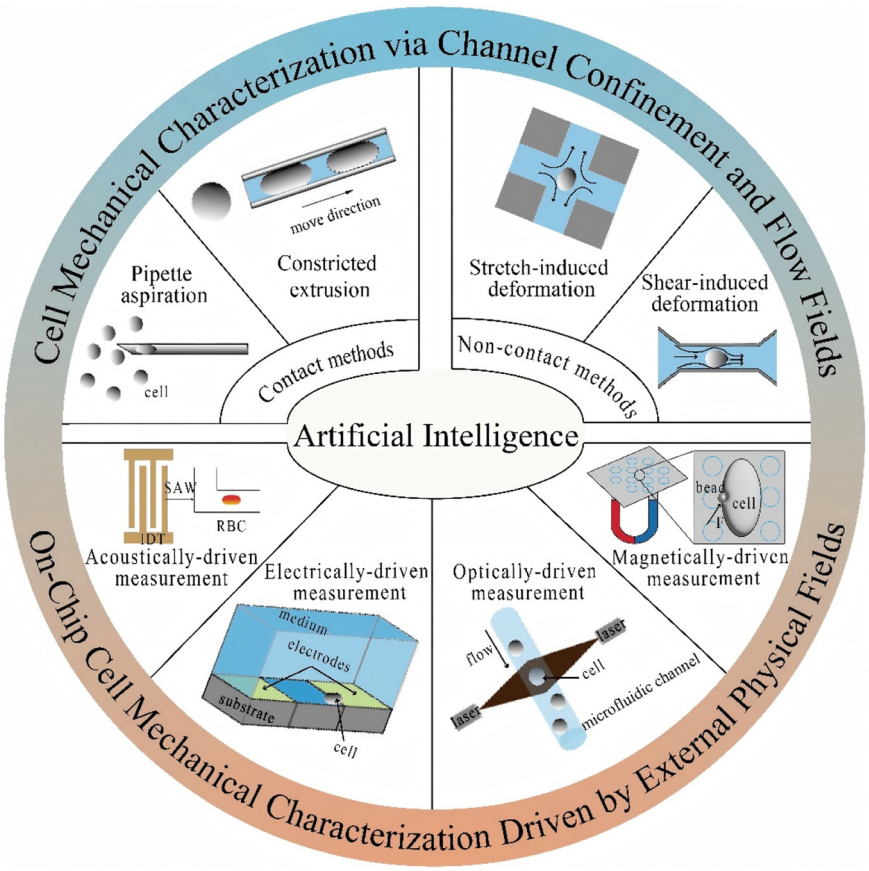

Fig. 1 Overview of the classifications and principles of single-cell mechanical characterization methods.

are being explored *via* AI-driven algorithms, such as a generalized predictive control (GPC) algorithm, for real-time parameter adjustment and iterative experimental optimization.[40] However, AI integration in on-chip cellular mechanics remains nascent, with most current implementations focused on image analysis and basic feedback control.[41] The development of fully intelligent, autonomous platforms is therefore essential to unlock real-time, adaptive, and comprehensive single-cell biomechanical profiling.

AI is poised to address critical challenges beyond the reach of conventional analysis. A pivotal opportunity lies in decoding cellular mechanical heterogeneity at an unprecedented scale.[42] Traditional analysis often relies on pre-defined gating strategies that may obscure novel subpopulations.[43] In contrast, unsupervised machine learning can autonomously discover mechanically distinct cell states from high-dimensional deformation data, revealing new biomarkers for disease diagnosis and therapeutic monitoring.[44,45] Furthermore, AI enables predictive mechanophenotyping by learning direct, non-linear mappings from complex deformation dynamics to intrinsic properties, circumventing the need for simplified theoretical models that may not capture full cellular complexity.[46] These prospective applications underscore AI's potential not merely as a tool for acceleration, but as a catalyst for fundamentally new scientific discovery in mechanobiology.

This review examines advancements in microfluidic platforms for cellular mechanical characterization, tracing the evolution from conventional fluid-driven methods to approaches employing external physical fields, and emphasizing the pivotal and transformative impact of AI within every methodological category discussed (Fig. 1). We begin by discussing conventional microfluidic techniques, including contact methods such as constricted extrusion and pipette aspiration, as well as non-contact methods like shear-induced and stretch-induced deformation. The discussion then shifts to a new paradigm enabled by external physical fields, which provide distinct mechanisms for mechanical stimulation. Furthermore, we examine the emerging role of AI in automating the analysis of complex mechanical phenotyping data and optimizing experimental parameters. Finally, we outline future research directions in this interdisciplinary field, emphasizing the potential of intelligent microfluidic platforms to transform both fundamental biomechanical research and clinical diagnostics.

Cell mechanical characterization *via* channel confinement and flow fields

This section surveys microfluidic platforms for on-chip cell mechanical characterization that utilize channel confinement and fluid flow, emphasizing the critical integration of AI. It covers contact methods, such as constricted extrusion and pipette aspiration, where direct physical interaction with channel walls induces deformation, and non-contact methods (*e.g.*, shear/stretch-induced deformation), where shear or tensile flow fields probe cell mechanics.[47–50] We detail how AI substantially enhances these methods, from employing CNNs and Mask R-CNN for automated cell perception in constricted channels, to utilizing SVM for mechanophenotyping in flow-based assays, and applying deep neural networks for regressing mechanical properties from deformation data.[32,38,51–53] These concrete examples underscore AI's indispensable role in enabling high-throughput, precise, and automated analysis.

Contact methods

Constricted extrusion. The constricted extrusion technique employs microchannels with diameters marginally smaller than the target cells, inducing mechanical compression as cells traverse these narrow structures under fluidic propulsion. By tracking morphological alterations,[6,34,54] velocity variations,[55,56] passage time[57,58] and entry time,[59] key mechanical properties such as deformability,[6,19] elasticity[47] and viscoelasticity[60] can be inferred. These parameters delineate the cellular response to compressive stress during extrusion. Fundamental channel geometries for constricted extrusion are exemplified by Horade *et al.*,[34] who[34] used the geometrically constrained microfluidic channel to characterize cellular viscoelasticity (Fig. 2A). To dissect the spatiotemporal dynamics of cell–channel interactions, Hu *et al.*[60] designed a progressively constricting microchannel, enabling precise quantification of the onset and locus of cell–sidewall contact during squeezing. For high-throughput applications, parallelized microfluidic arrays have been developed (Fig. 2B).[61] Raj *et al.*[47] implemented a multi-parallel micro-constriction system that predicts cellular Young's modulus through theoretical modelling.

Despite advancements in parallelization, conventional analytical workflows for constricted extrusion data—such as manual tracking of cell deformation or parameter computation—remain time-intensive and susceptible to human error, impeding efficient translation to clinical contexts. The integration of AI has markedly advanced microfluidic systems, particularly in expediting cellular feature extraction and enhancing the precision of mechanical property quantification. AI-assisted analysis streamlines the detection of passage time and deformation metrics, addressing pivotal bottlenecks in high-throughput screening. Deep learning networks have been widely adopted for image segmentation and boundary detection in single-cell measurements: high-resolution cellular images processed *via* these algorithms enable automated recognition of cell contours, precise extraction of boundary information, and quantitative determination of geometric parameters (*e.g.*, diameter, roundness, and volume change). When coupled with physical models (*e.g.*, linear elasticity theory), these parameters facilitate the calculation of mechanical metrics such as Young's modulus, enabling end-

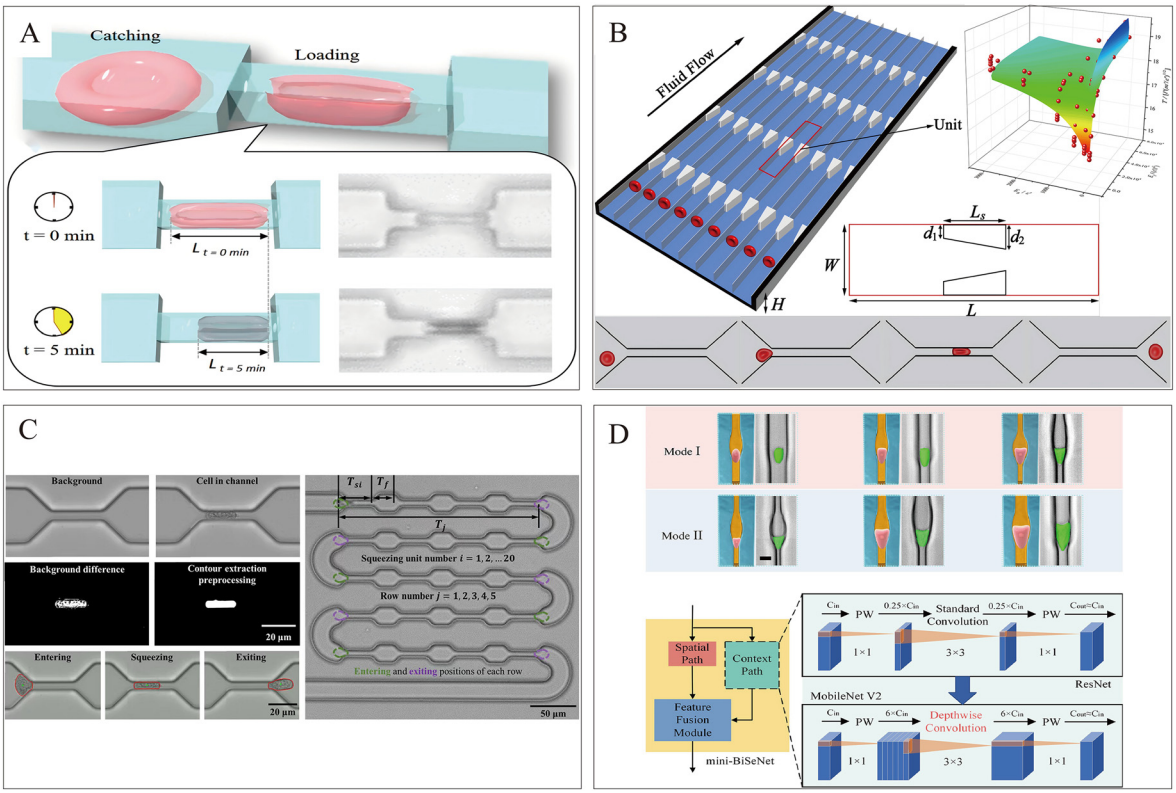

Fig. 2 Schematic diagrams of single-cell mechanical property measurement *via* constricted extrusion. (A) Schematic of cell extrusion and deformation through a narrow microfluidic channel. Reprinted with permission from ref. 34, under the terms of the Creative Commons CC BY license, *Micromachines*. (B) Schematic of the microfluidic device with multiple parallel micro-constrictions for characterization of mechanical properties of single cells. Reprinted with permission from ref. 61. Copyright 2019, Elsevier. (C) Automated obtainment of passage time assisted by computer vision under the microscope. Reprinted with permission from ref. 62. Copyright 2021, American Chemical Society. (D) Recognition of rapid cell deformation based on deep learning after squeezing and deforming cells using two different modes of fluidic channels, and optimized BiSeNet V1 by replacing ResNet with MobileNet V2 to develop a mini-BiSeNet. Reprinted with permission from ref. 63. Copyright 2023, Royal Society of Chemistry.

to-end automation from image acquisition to mechanical property output. Notably, Li *et al.*[62] demonstrated that computer vision-based automated compression time measurement, applied to cells traversing a serpentine microfluidic channel with five constriction rows, supported mechanical deformation analysis and cancer cell classification (Fig. 2C). This approach demonstrates the potential of AI-assisted extrusion cytometry not only as a research tool but also as a clinical diagnostic aid, for instance, in stratifying cancer patients based on the mechanical phenotypes of their circulating tumor cells (CTCs), which could inform prognosis and treatment selection. Similarly, Zhou *et al.*[63] developed a mini-bilateral segmentation network (mini-BiSeNet) to rapidly identify cells and extract deformation features, enabling the classification of distinct cell populations based on size and mechanical properties (Fig. 2D). They compare the differences between residual network (ResNet) and mobile network (MobileNet) V2 (where C_{in} and C_{out} are the number of input and output channels, respectively). Between the two pointwise (PW) convolutions, MobileNet V2 used the depthwise (DW) convolution.

Pipette aspiration. Pipette aspiration is a widely used technique for analysing cellular mechanical properties. It applies negative pressure through microtubes with diameters smaller than target cells to induce controlled deformation, thereby facilitating studies of deformation kinetics.[48] To measure membrane area compressibility modulus (K_a), the stress and strain at rupture (σ_L, α_L), and the energy required for failure (cohesive energy, E_c), Ibarboure *et al.*[64] employed micropipette aspiration to study giant unilamellar vesicles (Fig. 3A). Beyond single-pipette systems, dual micropipette configurations can quantify intercellular adhesion forces. For example, Plater *et al.*[65] applied this setup to assess the mechanical stability of mouse embryos, revealing that compaction enhances intercellular adhesion by enlarging the Cdh1 adhesion ring (Fig. 3B). This work underscores the potential of cell mechanical measurements as a novel, non-invasive biomarker for assessing embryo quality. By quantifying intercellular adhesion forces, such microfluidic pipette aspiration systems could be developed into diagnostic tools to aid in the selection of viable embryos for assisted reproductive technologies (ART), ultimately aiming to improve clinical success rates.

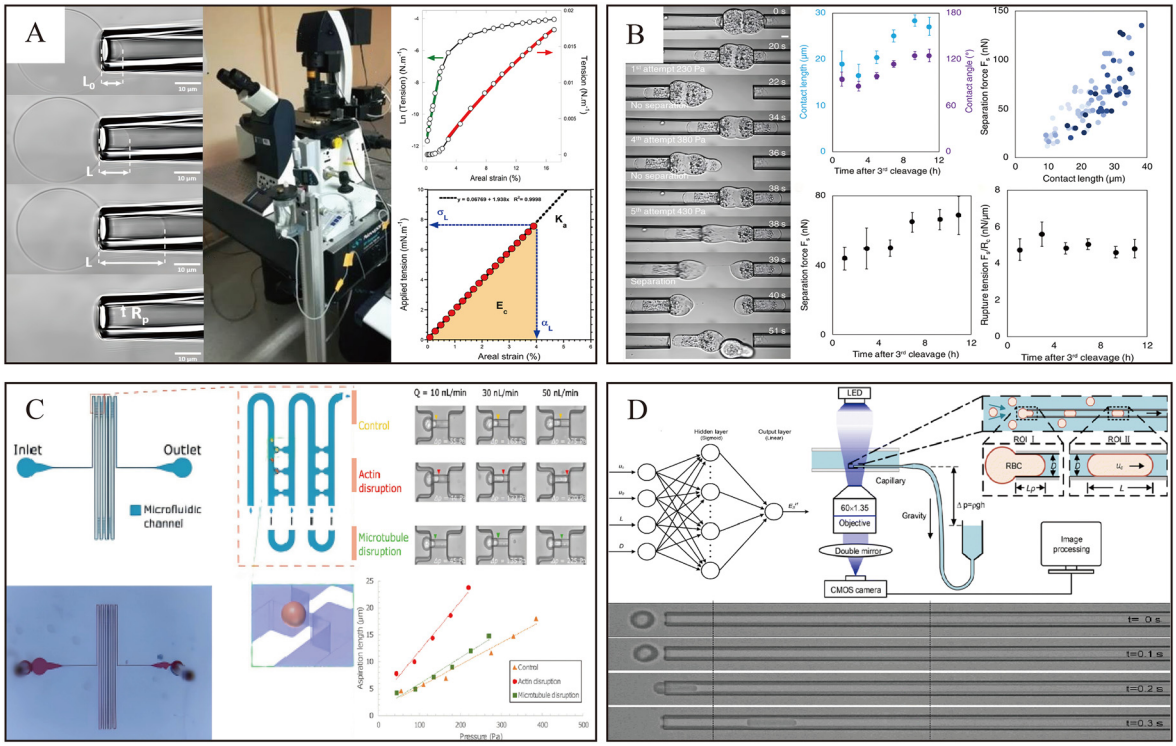

Fig. 3 Pipette-based microchannel for single-cell mechanical property characterization. (A) Micropipette aspiration system and stress–strain analysis of giant unilamellar vesicles (GUVs), showing the images of GUVs under varying suction pressures, the setup components, and representative stress–strain plots obtained in both the general aspiration and stretching regimes. Reprinted with permission from ref. 64. Copyright 2020, JoVE. (B) Mechanical coupling of compacting 8-cell stage doublets, showing time-lapse imaging of doublet separation using dual pipette aspiration, contact length and angle before separation, separation force measurements, and rupture tension throughout the 8-cell stage. Reprinted with permission from ref. 65, under the terms of the Creative Commons Attribution-NonCommercial-NoDerivs (CC BY-NC-ND 4.0), *Biophysical*. (C) General layout of a microfluidic microtubule aspiration array. An enlarged schematic illustrates the interface between the micropipette-aspiration unit and main channel, alongside a precise depiction of a cell residing on the aspiration unit. The inhalation length of MCF-7 cells in the three control groups is shown as a function of pressure. Reprinted with permission from ref. 48. Copyright 2020, AIP Publishing. (D) A three-layer BPNN for extracting shear modulus to accurately characterize the mechanical properties of erythrocytes, with input variables including u_0, u_c, L, and D, and output variable ESH. Reprinted with permission from ref. 67. Copyright 2024, Royal Society of Chemistry.

Similar to constricted extrusion methods, parallelized microcapillary arrays significantly enhance experimental throughput. Boot *et al.*[66] developed a microfluidic chip with multiple pockets under uniform suction pressure, enabling high-throughput measurement of viscoelastic deformation in cellular spheroids. Wu *et al.*[48] designed a microtubule array flow channel featuring a serpentine microfluidic channel and 42 micropipette-aspiration units (Fig. 3C). This system allows for the high-throughput capture of cells into predefined chambers, facilitating parallel analysis of mechanical properties, including Young's modulus, and transport phenomena.

Integrating machine learning with fluid–cell interaction analysis has further improved measurement precision for mechanical properties. Wei *et al.*[67] combined hydrodynamic mechanisms with a three-layer BPNN to accurately determine the membrane shear modulus, viscosity, surface area, and volume of individual RBCs (Fig. 3D). The precise quantification of RBCs' mechanical properties is crucial for understanding and diagnosing hematological disorders. For example, in hereditary spherocytosis and malaria, the loss of deformability is a key pathophysiological marker.[68,69] This method paves the way for developing microfluidic clinical analyzers for blood diseases, enabling accurate diagnosis and monitoring of treatment efficacy.

In addition to classical contact methods like constricted extrusion and pipette aspiration, measurement on micro- and nano-patterned substrates has emerged as a distinct contact-based approach for probing cellular mechanical properties.[70] These engineered surfaces use topographic and biochemical cues, such as micropillars, nanodiscs, or spatially organized extracellular matrix proteins, to control cell adhesion, spreading, and mechanotransduction with high precision.[71,72] Unlike methods that apply external forces directly, patterned substrates elicit intrinsic mechanical responses through spatial confinement and ligand presentation. Cells adhering to these structures generate contractile forces through their actin cytoskeleton. By measuring the resultant deflection of micropillars, cellular traction forces can be quantified directly at the single-cell

level. This strategy, while contact-mediated, minimizes active mechanical perturbation.[73] Recent work has demonstrated that nanoscale features, such as TiO_2 nanodiscs functionalized with Arg–Gly–Asp peptides, can regulate integrin clustering and downstream signaling events like YAP nuclear translocation in a diameter-dependent fashion, with 100 nm discs yielding optimal adhesion and spreading behavior.[71] Similarly, micropillar arrays have been employed to quantify cellular traction forces by measuring pillar deflection, enabling direct assessment of contractility at the single-cell level.[74–76] These platforms offer distinct advantages, including compatibility with high-resolution microscopy, scalability for high-throughput analysis, and reduced risk of cell damage compared to aspiration or compression-based techniques. While the autonomous design of patterned substrates using AI is still emerging, the quantitative image data they produce are well-suited for AI-driven analysis.[70] Future developments will likely leverage machine learning not only to predict optimal pattern geometries for directing cell function but also to autonomously extract subtle mechanical phenotypes, such as traction stress maps, spatiotemporal spreading dynamics, and nuclear mechanotransduction events, from high-content imaging data.[77] Thus, micropattern complements existing contact methodologies and holds significant potential for next-generation, AI-enhanced mechanobiology studies.

However, contact methods, such as pipette aspiration and constricted extrusion, provide high-force, well-defined deformations but introduce friction and potential cellular damage, particularly when aperture size approximates the cell diameter.[78,79] Over-compression can lead to cell rupture, compromising measurement accuracy.[80] This can lead to an overestimation of cell stiffness and obscure native mechanical properties. Rational design of microfluidic channel dimensions is thus critical to minimize cellular stress and ensure reliable results. In contrast, non-contact techniques probe cells in near-physiological conditions, preserving viability.[81]

Non-contact methods

Non-contact techniques have emerged as a robust alternative to mitigate cellular damage associated with traditional contact methods, preserving cellular integrity while enabling high-precision mechanical property characterization. These approaches are broadly categorized into two primary strategies: shear-induced deformation and stretch-induced deformation, each leveraging distinct fluidic mechanisms to induce cellular deformation.

Shear-induced deformation. When a cell traverses a microfluidic channel with a diameter slightly larger than its own, it undergoes deformation driven by the combined effects of shear forces arising from the fluid's parabolic velocity profile and the applied fluid pressure gradient. The shear-induced deformation technique leverages laminar shear forces within microfluidic chips to apply controlled mechanical stress to cells, enabling quantification of key mechanical properties, such as deformability,[32,49,82,83] elasticity,[49,82,84] shear modulus,[85] viscosity,[85] and viscoelasticity,[86] by analysing morphological changes in the shear flow field. By minimizing direct cell–channel interactions, this non-contact approach reduces damage risk while closely mimicking the complex fluidic microenvironments cells encounter *in vivo*. Otto *et al.*[14] developed a high-throughput method for continuous mechanical characterization of large cell populations (>100 000 cells) by capturing images of cells deforming under shear gradients generated *via* fluid flow through microfluidic channels (Fig. 4A). The ability to mechanically profile thousands of cells within minutes opens up avenues for rapid diagnostic screening. This is particularly valuable for detecting mechanically altered cells in peripheral blood for early signs of metastatic progression or for monitoring patient response to therapy in near real-time, offering a powerful tool for cancer management. Another approach combining a convergent-divergent hyperbolic flow channel with microscopic tracking was introduced to investigate the dynamic behaviour of bioparticles under uniformly strained flow (Fig. 4B).[87,88]

Given the high-throughput capabilities of shear-induced deformation, manual data analysis is impractical, requiring the integration of AI for efficient data processing and interpretation. Combs *et al.*[32] designed a microfluidic system that subjects cells to repetitive deformation and relaxation under shear forces. Their analysis pipeline utilized MASK-RCNN to segment individual cells from high-speed video frames. The resulting time series of cell shapes were then analyzed using a sequence-based deep learning model (a CNN-gated recurrent unit (GRU) architecture), which automated dynamic feature extraction and significantly enhanced classification accuracy compared to traditional methods (Fig. 4C). Nguyen *et al.*[51] further advanced this field by establishing a framework that integrates fluid–structure interaction (FSI) with machine learning to predict single-cell mechanics. By generating realistic deformation data through FSI simulations, they enabled CNNs to learn the mapping from a cell's static deformed shape (two-dimensional (2D) image or three-dimensional (3D) coordinates) to its underlying membrane stiffness (Fig. 4D).

Stretch-induced deformation. Stretch-induced deformation employs a specialized microfluidic design, where a tensile flow field—generated by the convergence of two identical fluid streams in a cross-shaped channel—applies uniaxial tensile stress to cells, inducing elongation along the flow direction. Under this stress, cells stretch along the flow field direction. By monitoring morphological changes, elongation, and recovery during stretching, key mechanical properties such as deformability,[89,90] elasticity,[50] toughness, and viscoelasticity[50,91] can be comprehensively assessed. This technique is particularly valuable for studying cellular mechanical behaviours under physiological or pathological conditions. For example, Armistead *et al.*[11]

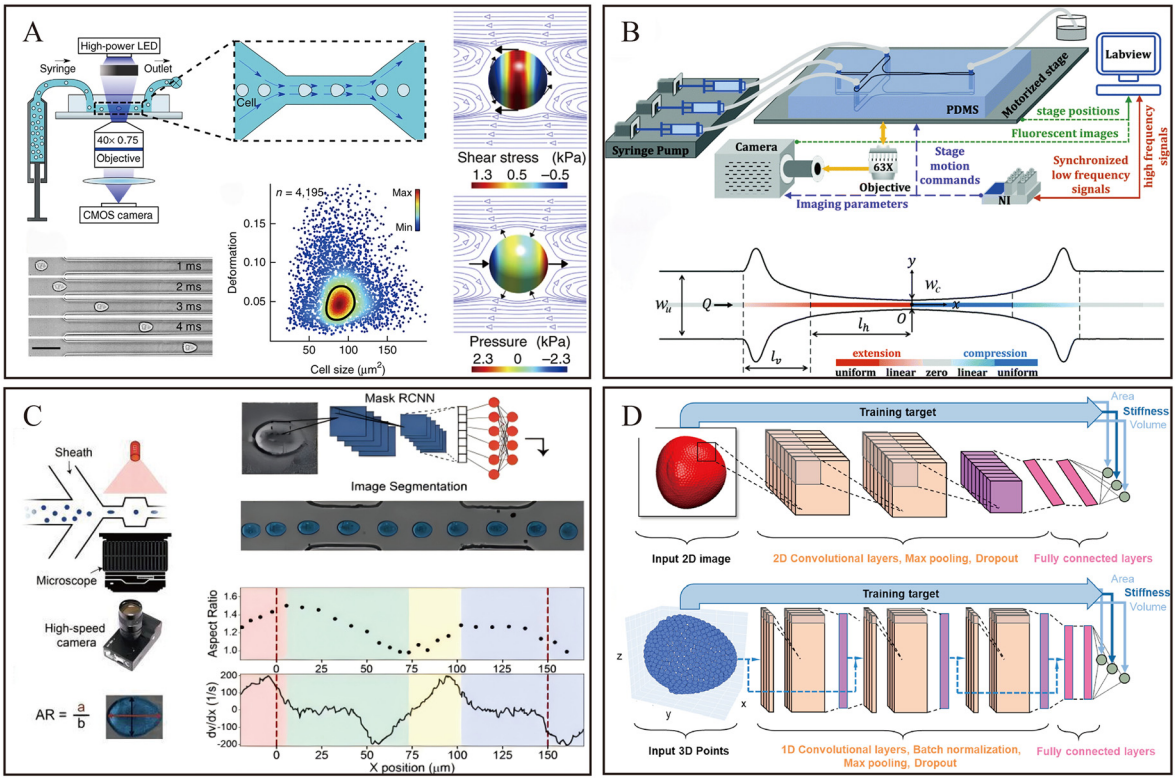

Fig. 4 Shear-induced deformation in microfluidic channels. (A) Shear-induced deformation setup and measurement principles. A time series of a cell deforming through constriction, along with a scatter plot of deformation *versus* cell size (cross-sectional area) for 4195 cells (points) acquired over 45 seconds. The simulation schematic shows the shear stress and pressure on the cell surface in the contracted region. Reprinted with permission from ref. 14. Copyright 2015, Springer Nature. (B) A detailed sketch of the optimized microfluidic convergent-divergent hyperbolic flow channel experimental device, showcasing the microfluidic channels, flow control, and tracking systems. Reprinted with permission from ref. 87. Copyright 2020, Royal Society of Chemistry. (C) Repetition of the principles of mechanical fractionation. The microfluidic channel contains a cavity between two narrow regions, with images captured by a high-speed camera. Cell boundaries were detected and fitted using MASK-RCNN, and deformation was quantified as the ratio of the two ellipse axes. Reprinted with permission from ref. 32, under the terms of the Creative Commons CC BY license, AIP Publishing. (D) Architectures of 2D-CNN and 3D-CNN models of a deformed capsule in a shear flow deformability cytometry. Reprinted with permission from ref. 51. Copyright 2023, Elsevier.

designed a cross-shaped tensile flow microfluidic channel to extract multiple parameters, including elastic modulus, plasticity, and size-normalized deformation indices, by tracking the deformation and relaxation of leukemia and colorectal cancer cells (Fig. 5A). By revealing distinct mechanical signatures of leukemia subtypes or colorectal cancer cell lines with varying metastatic potential, this stretch-based assays provide a physical biomarker platform that could complement conventional cytology in cancer diagnosis and mechanistic studies of metastasis, potentially guiding personalized treatment strategies. Gossett *et al.*[92] developed an automated microfluidic platform that probes single-cell deformability at high throughput (~2000 cells per s) using inertial focusing and stretch-induced deformation, enabling unbiased analysis of cell mechanics for applications in disease prediction, stem cell differentiation, and clinical diagnostics (Fig. 5B).

The integration of AI into stretch-induced deformation techniques has significantly enhanced the throughput and efficiency of microfluidic systems. For instance, Dudani *et al.*[93,94] introduced a hydrodynamic stretching method that avoids flow stagnation limitations by squeezing cells in vertical cross-flow, achieving a throughput of 65 000 cells per s in a polydimethylsiloxane (PDMS)-based microfluidic device (Fig. 5C). High-speed CMOS cameras captured stretched cells, and a shape extraction algorithm based on polar-to-Cartesian mapping was implemented in a diagnostic system to quantify cell deformation and extract key mechanical parameters from image sequences. This approach quantified the cell's deformability at the initial moment of stretching (D_{HA,t_i}) and its maximum deformability during the pinched-flow phase ($D_{HA,max}$), as well as in a subsequent in-line extensional flow (D_{DC,t_i} and $D_{DC,max}$). These parameters enabled the differentiation of cell populations based on their transient and peak mechanical responses to different types of stress. Deng *et al.*[33] proposed an inertial microfluidic cell stretcher (iMCS) for near real-time deformability characterization of large cell populations (Fig. 5D). This platform automates the entire mechanotyping process through a computer vision-based approach, implemented with a custom algorithm using the OpenCV library. This method enabled the real-

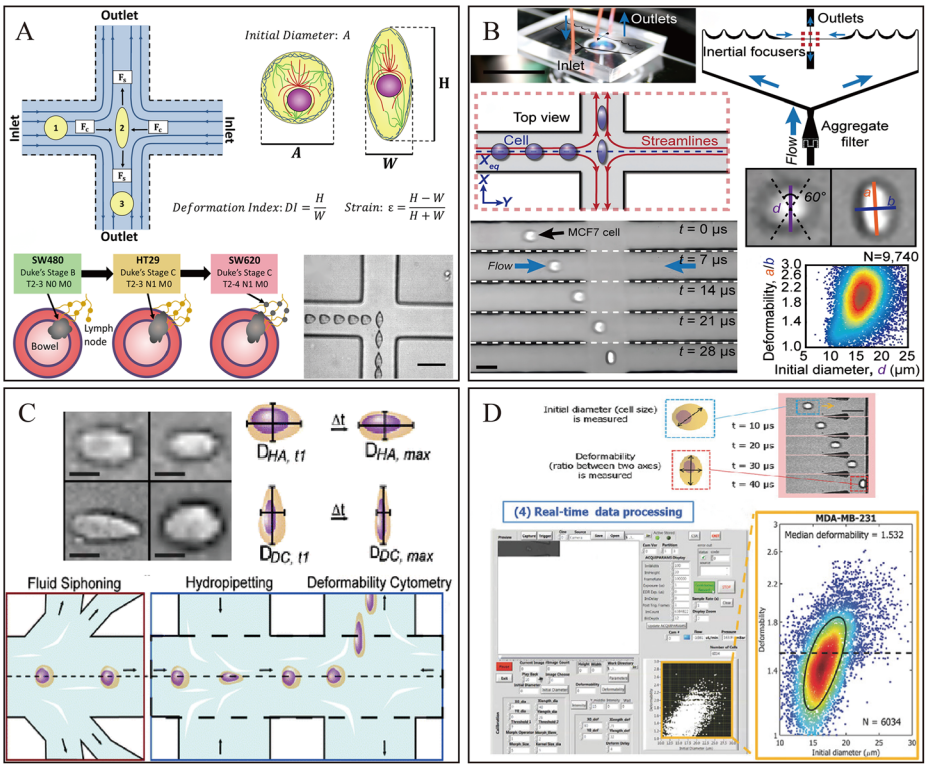

Fig. 5 Deformation of microfluidic channels induced by fluid stretching. (A) Schematic diagram of the cross-flow zone, the overall cell, and the colorectal cancer models of three cell lines: SW480, HT20, and SW620. The superimposed bright-field images show a single cell entering (from left) the stagnation point (SP) of the extensional flow device and exiting to the bottom of the chamber. Reprinted with permission from ref. 11. Copyright 2020, Springer Nature. (B) Schematic diagram of microscope installation and fluid-coupled microfluidic deformation cytometry device. Cells can enter the elongational flow from two directions. High-speed microscope images demonstrate the schematic deformation of cells as they align to the center of the elongational flow at the inertial focusing position. Reprinted with permission from ref. 92. Copyright 2012, Royal Society of Chemistry. (C) Pinched-flow hydrodynamic stretching of single cells. Reprinted with permission from ref. 93. Copyright 2013, Royal Society of Chemistry. (D) High-speed microscopy images and control panel screenshots of the cell deformation process and mechanical characterization of MDA-MB-231 cells. Reprinted with permission from ref. 33. Copyright 2017, Wiley.

time quantification of mechanical properties (*e.g.*, shear modulus) by automatically tracking cells and calculating their initial diameter and deformability from high-speed image sequences. Lin *et al.*[95] introduced multi-parameter deformability cytometry (m-DC), which extracts over 20 physical phenotype parameters, including size, deformability, deformation kinetics, and morphology, enabling high-throughput characterization of pluripotent cells and their derivatives. SVM was integrated to enhance the stability and reliability of parameter extraction.

The fundamental difference from contact methods lies in the force application mechanism. Non-contact approaches measure cell deformability without wall effects, capturing properties like cortical tension that are often masked in constriction-based assays.[96–98] However, the resulting data streams are typically noisier and higher-dimensional (*e.g.*, dynamic deformation videos, multi-parametric field responses).[99] This is where AI becomes indispensable. Manual analysis is impractical, and traditional models fail to capture the non-linear mechanics. Machine learning, particularly DNN, excels at extracting robust features from these complex datasets, directly mapping raw image or signal data to mechanical properties, thereby bridging the interpretability gap between contact and non-contact measurements.[100]

On-chip cell mechanical characterization driven by external physical fields

Electrically-driven measurement

Electrically-driven measurement leverages electric fields to manipulate cells in a non-contact manner, utilizing microchannels and electrode structures integrated into microfluidic chips to capture, stretch, and deform cells, enabling the assessment of their mechanical properties.[101–103] This approach is mainly based on dielectrophoresis (DEP), where cells are deformed or displaced in an electric field due to differences in their dielectric properties.[21] Qiang *et al.*[104] introduced a method for characterizing the mechanical fatigue of individual cells using amplitude-modulated electrode formation combined with microfluidics (Fig. 6A). This technique subjects cells to

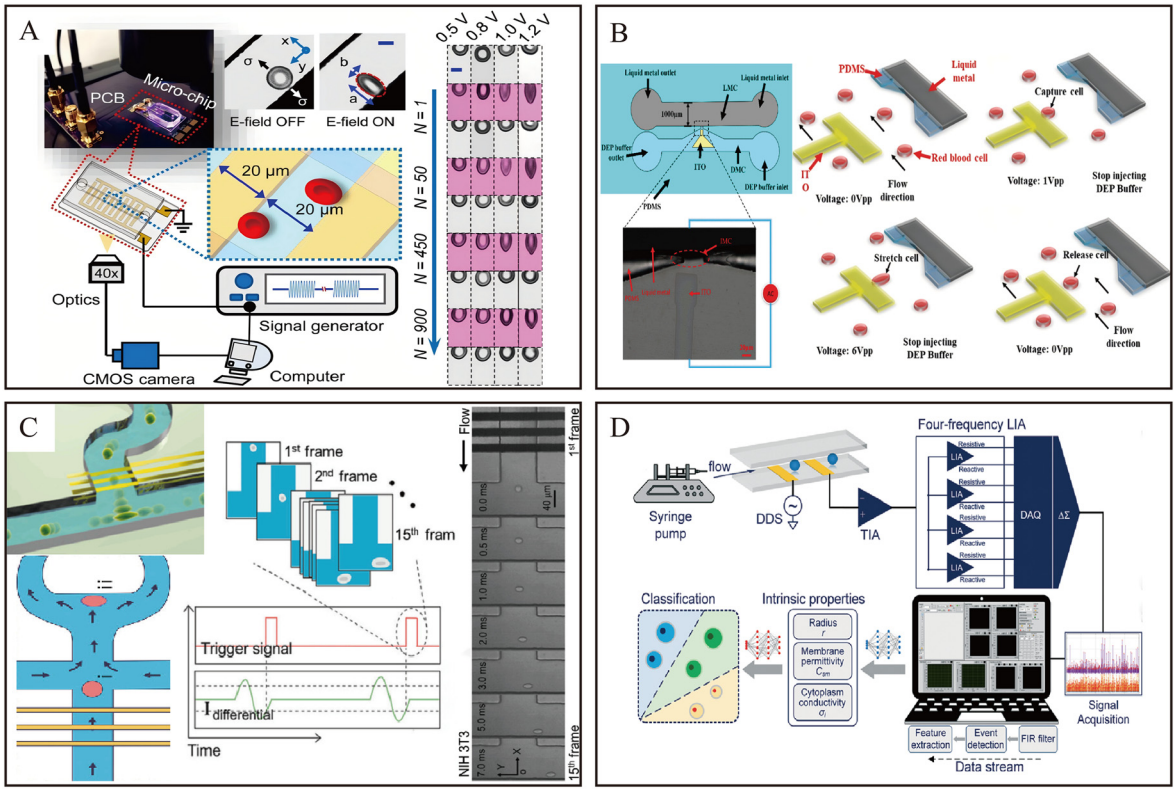

Fig. 6 Electrically-driven deformation in microfluidic channels. (A) Experimental setup for fatigue testing of single RBCs using amplitude-modulated electrodeformation and microscopic images of cell deformation measured in real time in a microfluidic chip. Reprinted with permission from ref. 104. Copyright 2019, under the terms of the Creative Commons Attribution-NonCommercial-NoDerivatives License 4.0 (CC BY-NC-ND), *PNAS*. (B) Schematic diagram of a microfluidic chip consisting of liquid metal ITO electrode and the on-chip cell stretching process. When no voltage was applied, cells flowed forward along the microchannels; the microfluidic syringe pump was stopped, and erythrocytes were captured with a sinusoidal waveform at 1 Vpp and a frequency of 1.5 MHz; the voltage was increased to stretch the cells. Reprinted with permission from ref. 109. Copyright 2019, under the terms of the Creative Commons license 4.0, IEEE. (C) Microfluidic system for high-throughput cytomechanical phenotyping. Dynamic deformation of a single cell is shown. When the camera was triggered, 15 frames were recorded for cell deformation analysis. Reprinted with permission from ref. 52 and 53. Copyright 2021, American Chemical Society and Copyright 2022, Wiley. (D) Overview of the RT-IFC framework using the principle of four-frequency lock-in amplifier and neural network for intrinsic characterization. Reprinted with permission from ref. 111. Copyright 2022, Royal Society of Chemistry.

prolonged static loading or controlled mechanical fatigue cycles, systematically measuring changes in morphological and biomechanical properties, particularly in RBCs and their membrane mechanics. Characterizing the mechanical fatigue of RBCs is directly relevant to understanding hemolytic anemias and improving the shelf life of stored blood for transfusions.[105] Thus, DEP-based platforms could thus find application in blood bank quality control and the study of RBCs membrane disorders, directly addressing clinical needs in hematology.[106] Hu *et al.*[107,108] developed a high-throughput Wheatstone bridge-inspired microfluidic device for single-cell mechanical characterization. Conventional DEP electrodes, typically made of indium tin oxide (ITO), gold, or platinum, have inherent limitations. Zhu *et al.*[109] pioneered the use of galinstan alloy liquid metal as a microelectrode to generate non-uniform electric fields for erythrocyte trapping and stretching (Fig. 6B). In their design, the liquid metal microchannel (LMC) housed the conductive electrode, while the adjacent DEP buffer microchannel (DMC) carried the cell suspension. This liquid metal electrode is cost-effective, easy to fabricate, voltage-stable, and reusable.

Electric fields in microfluidics directly manipulate cells without physical contact, minimizing cellular damage and ensuring measurement accuracy.[101] Integration with automated control systems and image analysis algorithms further reduces human error and enables fully automated measurements. Yang *et al.*[110] proposed a DEP-based platform integrating microfluidics with AI-driven automation, which not only enabled efficient acquisition of cellular mechanical data but also addressed low-throughput bottlenecks by automating data processing. Liang *et al.*[52,53] developed a microfluidic system for hydrodynamic stretching of cells in viscoelastic fluids, enabling high-throughput mechanical phenotyping (Fig. 6C). The subsequent cell type classification was performed using an SVM with a radial basis function kernel, which effectively distinguished different breast cancer cell lines based on their intrinsic deformability and size.

An electrical sensing unit detects cell arrival and triggers a high-speed camera to capture images, from which mechanical phenotypes such as cell size and deformability are extracted. Feng *et al.*[111] advanced the field with a neural network-enhanced impedance flow cytometry method (Fig. 6D). Their system integrated key hardware modules, including a transimpedance amplifier (TIA), a direct digital synthesis (DDS) source, a lock-in amplifier (LIA), and a data acquisition (DAQ) unit, to accurately measure single-cell impedance. These measurements were processed in real-time by 2 deep fully connected neural networks (FCNs) that regressed intrinsic biophysical properties and performed cell classification, enabling high-throughput, real-time intrinsic characterization with a 10 000-fold improvement in speed.

Optically-driven measurement

Optically-driven measurement of cellular mechanical properties is an advanced approach that combines optical and microfluidic technologies, enabling non-contact, high-precision characterization of cells at the microscale. Modern optically-driven microfluidics employs focused laser beams to generate optical forces that non-invasively stretch or deform cells within microfluidic channels. By analysing cellular deformation responses through high-speed imaging, key mechanical properties such as elasticity and viscosity can be precisely quantified.[112]

The evolution of optically-driven microfluidics has progressed from early mechanical cell manipulation methods to sophisticated non-contact techniques, overcoming limitations such as cellular damage while enabling high-throughput and precise mechanical property measurements. Lee *et al.*[113] proposed an on-chip method to test RBCs deformation under optical pressure, where a low numerical aperture (NA) was utilized to push and deform cells, thereby enhancing sensitivity in detecting cancerous diseases (Fig. 7A). Building on this work, Roth *et al.*[114] developed a linear optical stretcher for high-throughput assessment of cellular mechanical properties. By precisely controlling laser beam distribution and intensity, this method forms optical traps based on two Gaussian intensity distributions, enabling *in situ* capture and stretching of suspended cells.[115] Analysis

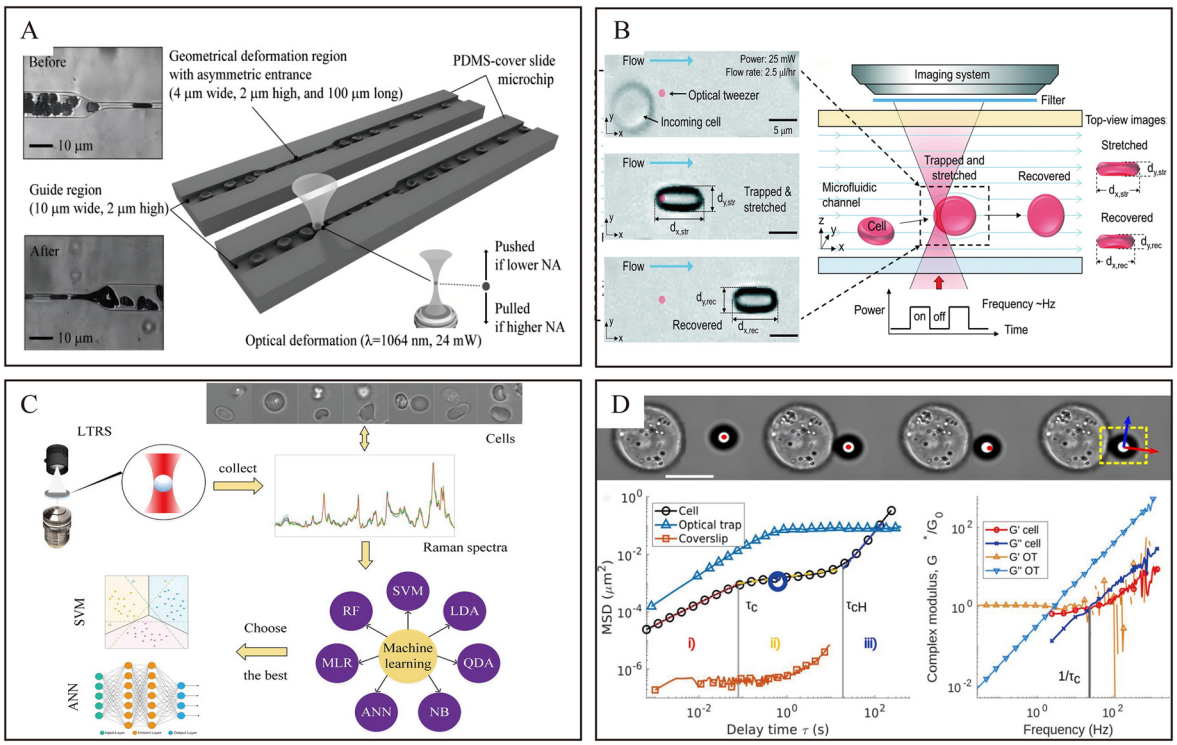

Fig. 7 Optically-driven deformation in microfluidic channels. (A) Schematic illustration of on-chip erythrocyte deformability test under optical pressure. The insets show the erythrocytes before and after the deformation region, respectively. Reprinted with permission from ref. 113. Copyright 2007, Royal Society of Chemistry. (B) Schematic of the principle and the implementation of the optofluidic "tweeze-and-drag" cell stretcher, and a linear spring model for the mechanical response of a cell under a stretching force. Reprinted with permission from ref. 117, under a Creative Commons Attribution-NonCommercial 3.0 Unported Licence, Royal Society of Chemistry. (C) Single-cell laser optical tweezers Raman spectroscopy system. Seven machine learning classification models are analysed and compared based on classification accuracy, precision and recall metrics. Reprinted with permission from ref. 120. Copyright 2022, Elsevier. (D) The entire process of bead–cell interaction was analysed using thresholding and centering methods to generate the position-time trajectory of the bead, resulting in the mean square displacement (MSD) data for beads in three different states. The normalized complex modulus of the cell and optical tweezers was then calculated using the Fourier transform of the normalized MSD. Reprinted with permission from ref. 121. Copyright 2023, under the terms of the Creative Commons CC-BY license, Elsevier.

of cellular deformation and displacement allows for the assessment of their mechanical properties.[116]

Another prominent optical method for single-cell deformability detection is optical tweezers (OT). Unlike optical stretchers, which use weakly diverging counter-propagating beams, OT employs strongly focused laser beams to perform precise measurements at specific cellular sites.[22] Yao *et al.*[117] utilized periodically chopped, tightly focused laser beams as optical tweezers to temporarily trap cells, while flow-induced drag stretched the cells laterally within a microfluidic channel (Fig. 7B). In contrast, Sawetzki *et al.*[118] directly stretched cells and investigated changes in mechanical properties of RBCs caused by *Plasmodium falciparum* infection, establishing dynamic viscoelasticity as a foundation for non-destructive mechanical phenotyping in high-throughput cell classification. The non-invasive nature of optical stretching makes it ideal for monitoring subtle changes in cell mechanics upon drug treatment or pathogenic infection. Quantifying the increase in RBCs' rigidity upon Plasmodium falciparum infection provides a direct measure of malaria disease progression and could be used to screen for anti-malarial compounds, bridging the gap between basic research and therapeutic development. In an alternative approach, Yousafzai *et al.*[119] introduced an OT technique for cell indentation at piconewton (pN) forces, where cells are axially moved against trapped microbeads, and bead displacement serves as a direct indicator of cellular interaction, eliminating potential interference from trap drift.

The integration of AI has significantly enhanced the precision, accuracy, and processing speed of Raman spectroscopy, strengthening its utility for characterizing cellular mechanical properties in optically-driven microfluidics. Raman spectroscopy, often referred to as a "fingerprint" spectrum, is a robust technique for characterizing biological and chemical samples. Liu *et al.*[120] developed a single-cell laser optical tweezer Raman spectroscopy (LTRS) system (Fig. 7C), where spectral features, including frequency shifts, were extracted using the Boruta algorithm. These shifts reflect mechanical properties such as stress and strain, enabling indirect characterization of elastic modulus. Seven machine learning models were compared based on classification accuracy, precision, and recall.

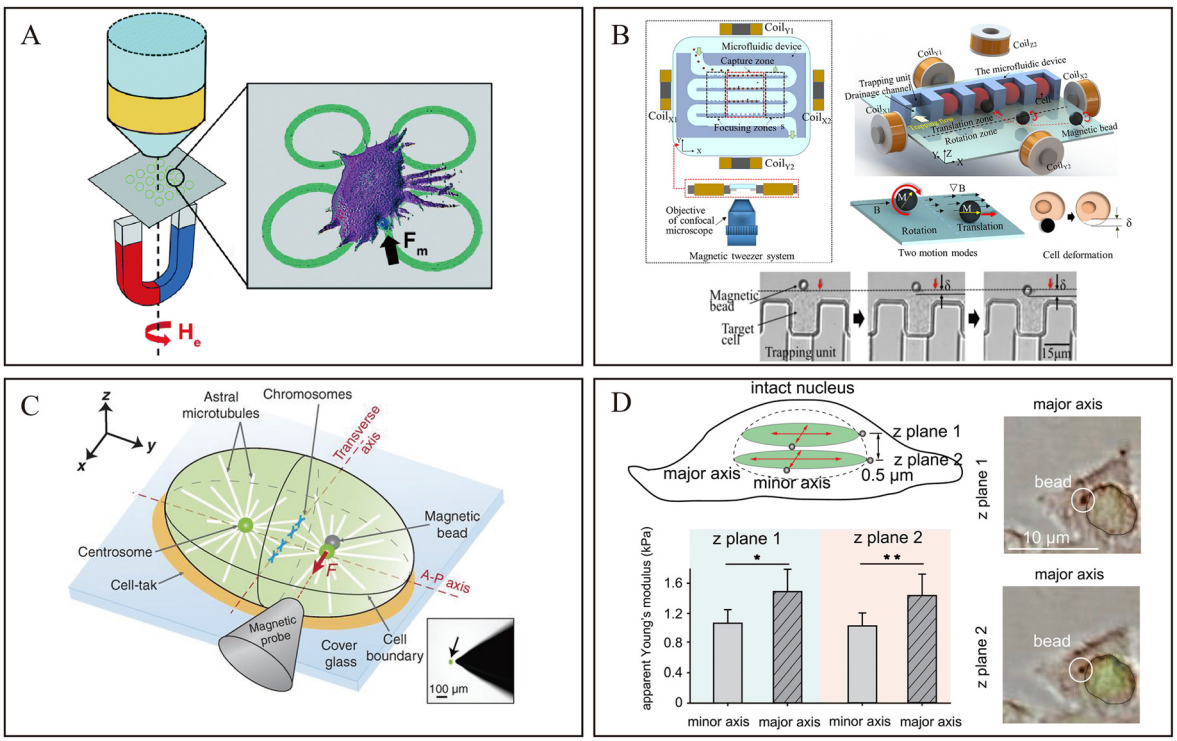

Fig. 8 Magnetically-driven deformation in microfluidic channels. (A) The schematic of the experimental setup illustrates a ring-shaped ferromagnetic nanostructures on a chip. The device operates by applying a magnetic force (Fm) to the cell membrane of HeLa cells cultured on the chip surface. Reprinted with permission from ref. 123. Copyright 2016, Royal Society of Chemistry. (B) A 2D and 3D magnetic tweezer system based on a high-efficiency microfluidic device under confocal microscopy, along with moving schematic of magnetic bead rotation mode in constant magnetic flux density and translation mode in magnetic gradient, as well as cell deformation under bead-induced extrusion force. Reprinted with permission from ref. 23. Copyright 2021, IEEE. (C) Spindle centering force measurement with magnetic tweezers: A *C. elegans* embryo (green) was immobilized on a cover glass *via* Cell-Tak (orange); a superparamagnetic bead was placed in the astral microtubule array for force application. Reprinted with permission from ref. 124. Copyright 2016, Science. (D) Nuclear mechanics polarity across *Z* planes: Schematic of measurements along the nucleus' major and minor axes in two *Z* planes; representative images with bead locations marked; results showing greater stiffness along the major axis in both planes. Reprinted with permission from ref. 40. Copyright 2019, Science.

Hardiman *et al.*[121] applied a minimally invasive passive micro-rheological technique by attaching a bead to the cell surface (Fig. 7D). The bead's motion was recorded and analyzed through thresholding and centroiding, a deterministic image processing approach. The trajectories were used to quantify the cell's low-frequency elastic modulus (G_0) and dynamic mechanical changes, including the plateau onset time (τ_c), its inverse ($1/\tau_c$) as the frequency domain, and the superdiffuse motion onset time (τ_{ch}).

Magnetically-driven measurement

Magnetically-driven measurement utilizes magnetic particles for cellular positioning and manipulation. By exploiting interactions between external magnetic fields and magnetic materials (*e.g.*, magnetic beads), applied magnetic forces indirectly induce cellular deformation—enabling precise quantification of mechanical properties such as stiffness, elasticity, and viscoelasticity.[122]

Magnetic tweezers (MT) are a widely used method in magnetically-driven measurement. MT employs magnetized particles (beads) attached to a cell surface or membrane. By manipulating the magnetic field, forces ranging from piconewtons to nanonewtons can be applied, indirectly inducing mechanical deformation in the target cell. Monticelli *et al.*[123] developed a chip-based device utilizing a magnetic domain wall manipulator, enabling the precise application of localized forces to living cells (Fig. 8A). By manipulating superparamagnetic beads, a magnetic force of several hundred piconewtons (pN) was applied to the HeLa cell membrane, inducing localized deformation. This deformation was quantitatively analysed through experimental measurements and computational simulations. In contrast, Tang *et al.*[23] integrated MT into a high-efficiency cell-aligned microfluidic device, demonstrating two modes of magnetic bead motion under a pulsed electromagnetic field to assess single-cell mechanical properties (Fig. 8B). They physically compressed HeLa and C2C12 cells arranged in the microfluidic device using MT to measure cell stiffness.

Extending beyond extracellular mechanical property assessment, magnetic tweezers have been employed to investigate intracellular mechanical dynamics. Garzon-Coral *et al.*[124] used magnetic tweezers to exert calibrated forces (up to 200 pN) on mitotic spindles in *Caenorhabditis elegans* embryos, investigating the force-generating machinery that maintains spindle position during cell division (Fig. 8C). This machinery exhibits viscoelastic properties, with centering stiffness increasing fivefold from metaphase to anaphase and scaling with the number of astral microtubules, providing direct measurements of the forces governing intracellular structural dynamics during division. Wang *et al.*[40] further advanced such applications with a multipole magnetic tweezers system capable of submicrometer 3D positioning (average error 0.4 μm) and piconewton force control (up to 60 pN with 4 pN resolution) of submicrometer magnetic beads inside intact cells, enabling precise characterization of nuclear mechanical properties (Fig. 8D). Notably, this system integrated a GPC algorithm to address the low bandwidth of confocal imaging feedback, enhancing control accuracy for quantifying nuclear mechanical polarity (higher stiffness along the major axis) and force-induced nuclear stiffening.

Acoustically-driven measurement

Acoustically-driven measurement of cellular mechanical properties leverages the propagation and interaction of acoustic waves within microfluidic environments to apply acoustic pressure or radiation forces to cells, enabling the observation and analysis of cellular deformation and responses under acoustic fields.[125] This approach achieves the non-contact manipulation under an acoustic field and the high-precision control by microfluidics, offering a novel method for characterizing cellular mechanical properties.[126,127]

Five primary techniques are employed in acoustofluidic systems: bulk acoustic waves (BAW), surface acoustic waves (SAW), single-beam acoustic tweezers (SBAT), acoustic force spectroscopy (AFS), and bubble techniques. Augustsson *et al.*[126] introduced a balanced iso-acoustic focusing method based on BAW to analyse the effective acoustic impedance of single cells in continuous flow (Fig. 9A). A. Link and Franke[28] demonstrated an SAW-based microfluidic device that generates stationary acoustic fields to investigate static and dynamic deformation of erythrocytes under progressively increasing and oscillating acoustic fields. Wu *et al.*[128] developed a high-throughput microfluidic compressibility cytometry method using multi-tilt-angle SAW, enabling thousands of single-cell compressibility measurements within minutes by balancing acoustic and flow rates (Fig. 9B). Lim *et al.*[129] proposed an automated SBAT-based method for cancer cell classification, providing objective and quantitative measurements of human breast cancer cell deformation. Acoustic compressibility has emerged as a sensitive label-free biomarker for cell state. Its application in distinguishing cancer cell types holds promise for liquid biopsy applications, where isolating and characterizing rare CTCs from blood acoustically could provide a non-invasive means for cancer diagnosis and monitoring, significantly impacting clinical oncology.[130] Nguyen *et al.*[24] utilized AFS to measure the dynamic viscoelastic properties of cells under varying conditions, enabling continuous measurement of complex shear modulus over extended periods. Xie *et al.*[131] introduced a technique based on acoustically driven bubbles to analyse the deformability of cells suspended in microfluidic devices (Fig. 9C).

While acoustically-driven methods enable high-throughput, non-contact cellular manipulation, the complexity of data generated—including dynamic deformation trajectories, multi-parametric acoustic responses, and high-dimensional cell trajectory datasets—has posed challenges for efficient processing and parameter optimization. To address these limitations, integration of AI into acoustically-driven microfluidics has emerged as a powerful strategy, simplifying

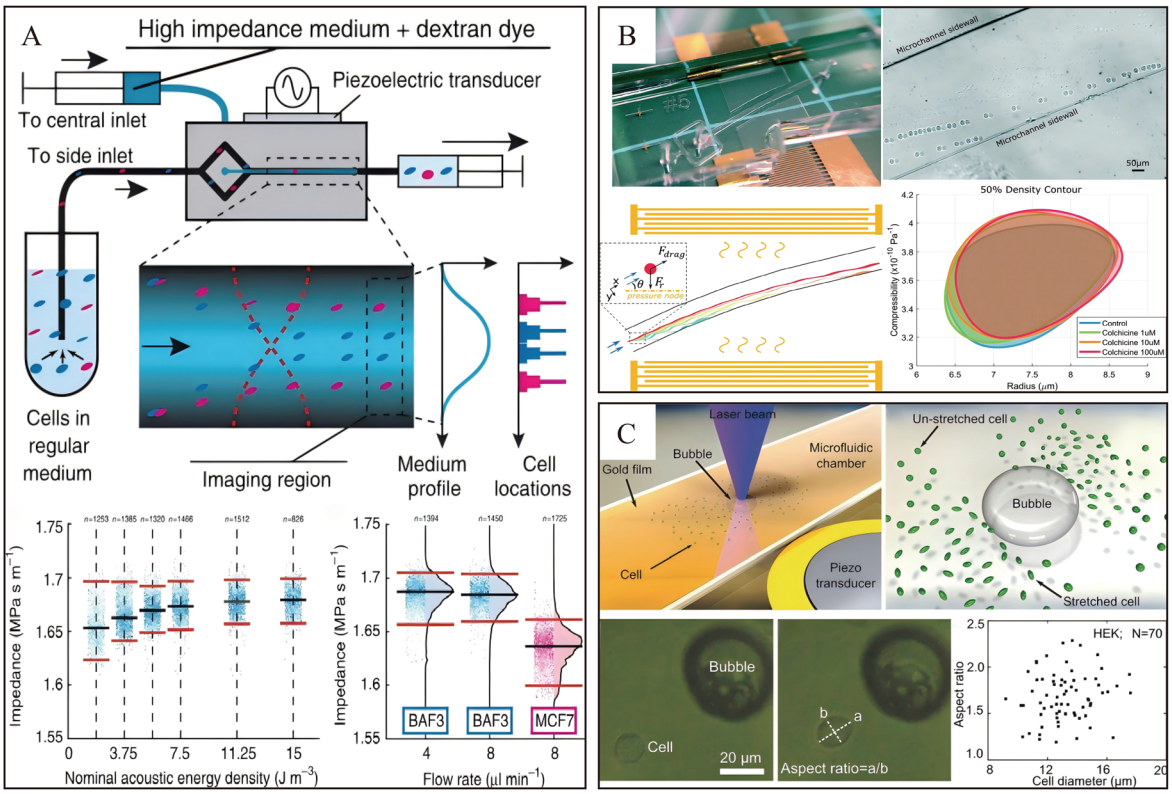

Fig. 9 Acoustically-driven deformation in microfluidic channels. (A) Schematic of iso-acoustic focusing cell measurements, accompanied by scatter plots of acoustic impedance (Zcell) for BA-F3 cells at six acoustic energy densities and flow rates of 4 μl min^{-1} and 8 μl min^{-1}, as well as for MCF7 cells at 8 μl min^{-1}. Reprinted with permission from ref. 126. Copyright 2016, under the terms of the Creative Commons Attribution 4.0 International License, *Nature*. (B) Photograph of the compressibility cytometer based on SAW, featuring a pair of interdigital transducers (IDTs) on a $LiNbO_3$ piezoelectric substrate and a PDMS microchannel with multiple segments inclined at varying angles. Reprinted with permission from ref. 128. Copyright 2021, Royal Society of Chemistry. (C) Schematic of the microfluidic chamber configuration, including the piezo transducer and cell stretching in the flow field around an acoustically activated oscillating bubble. Spherical suspension cells are stretched near the oscillating bubble, with a statistical analysis plot illustrating the deformability of HEK cell. Reprinted with permission from ref. 131. Copyright 2015, WILEY.

experimental workflows and optimizing technical parameters.[126,131,132] Guo *et al.*[133] combined real-time image processing with a geometric deformation algorithm to control and analyze cell stretching. Their data-driven method demonstrated that programmed high-frequency deformation is superior to continuous stretching for modulating membrane permeability. Rezayati Charan *et al.*[134] employed a diffuse image tracking method to measure cell trajectories in a homogeneous suspension medium, using neural networks to analyse and classify three-dimensional trajectories of thousands of single cells. As a non-contact force source, acoustic waves minimize mechanical damage to cells, preserving their integrity and activity. By precisely adjusting acoustic parameters, the magnitude and direction of acoustic pressure and radiation forces can be finely controlled, enabling precise cell manipulation.

Discussion and future directions

Mechanical characterization of cells enables the distinction and selection of specific cell types, as well as the differentiation between healthy and diseased cells, bypassing the need for biochemical assays.[135,136] In recent years, numerous devices based on diverse microfluidic principles have emerged, advancing the field to a stage where clinical translation is the next logical step.[26,137] However, several challenges hinder the transition of microfluidic methods from laboratory research to clinical practice. The reliable application of patient-derived samples and the management of complex data analysis remain significant barriers. Patient-derived cells often exhibit clustering and high adhesion, complicating single-cell analysis in microfluidic devices. For example, abnormal sickle-shaped RBCs show reduced deformability and increased adhesiveness compared to normal cells, leading to non-specific attachment and device clogging in high-throughput applications.[138,139] Additionally, current technologies rely on specific microstructures, limiting the flexibility and effectiveness of cell deformation.[133]

Convergence of multiple physical fields for precision cell mechanics

To address the limitations of traditional fluidic-only microdevices, external physical fields have become integral to

advancing mechanical characterization. These fields provide non-contact, tunable mechanisms for manipulating cells and inducing deformation, laying the groundwork for high-precision, high-throughput assays. Electric fields enable precise manipulation of cell positions and arrangements within microfluidic channels through dielectrophoresis and electrostatic actuation.[140] Electrical sensors can also directly capture cellular electrical signals, reflecting internal states and mechanical property changes.[141] Optical field-assisted methods record dynamic cell deformations on a millisecond timescale and enable automatic extraction of cell boundaries and shapes *via* image processing algorithms.[112] Magnetic field technology utilizes magnetic nanoparticles or microrobots to capture, localize, and precisely manipulate target cells. By applying a magnetic field gradient within a microfluidic chip, magnetic particles attached to cell surfaces enable the systematic measurement of mechanical responses.[142] Acoustic wave-based methods generate precise, controllable pressure pulses and microfluidic flows, enabling uniform, contact-free cell stimulation.[143] By adjusting acoustic field parameters, cells undergo quantifiable deformations, allowing the inference of mechanical properties such as rigidity and viscoelasticity.[144] In addition to single-physics-field-assisted techniques, an increasing number of studies have focused on integrating multiple physical fields for cellular characterization.[145] This approach enables simultaneous multi-parameter assessment and correction, enhancing measurement accuracy and providing a more comprehensive understanding of cellular properties.[146] These systems enhance measurement reliability through active cell positioning, directional force application (including compression, tension, and shear), and real-time response monitoring.[147,148]

AI solutions for cell-mechanics problems

By processing complex datasets (*e.g.*, high-speed deformation images, multi-parametric sensor readings), AI algorithms extract nuanced mechanical phenotypes. Recent advances in image analysis software and deep learning have, for instance, enabled real-time evaluation of mechanical properties by autonomously identifying cell boundaries, tracking dynamic deformations, and correlating these features with stiffness or viscoelasticity—functions that extend beyond basic automation to intelligent interpretation.[149,150] Notable refinements in measurement resolution highlight this synergy: differential displacement measurements within two-stage spring systems, paired with on-chip microfabricated squeezers, now achieve nanoscale resolution (~10 nm) for large deformations.[151,152] Similarly, sensor-integrated microfluidic platforms, combined with advanced displacement techniques like sampling moiré, have improved data accuracy.[153] In such systems, AI further optimizes performance by refining force application parameters based on real-time sensor feedback, bridging the gap between automated data collection and intelligent decision-making.

Looking ahead, by integrating external physical fields with AI, we can move beyond incremental improvements and confront the basic cell-mechanics questions that conventional analyses still fail to resolve.[154] This integration enables a shift from descriptive mechanotyping towards predictive and mechanistic understanding.[155] By processing high-dimensional datasets, such as dynamic deformation videos and multi-parametric sensor readings, deep learning networks can extract spatiotemporal features that capture a cell's mechanical memory and transient adaptive states.[156,157] This capability moves characterization beyond static parameters like stiffness, allowing observation of cytoskeletal remodeling and stress relaxation kinetics at an unprecedented scale. Furthermore, unsupervised machine learning autonomously discovers novel mechanophenotypes from complex deformation data without pre-defined gating, revealing functionally distinct cell subpopulations that may be critical in tumor heterogeneity or therapy resistance.[158,159] Concurrently, embedding physical laws into neural network architectures facilitates the regression of intrinsic mechanical properties directly from raw imaging data, circumventing simplified theoretical models.[160] The emerging paradigm thus positions AI not merely as an analytical tool, but as an integral component of the experimental framework, capable of decoding the complex, non-linear mappings between molecular activity and mechanical output.[46] This progression promises to unlock real-time, adaptive, and comprehensive single-cell biomechanical profiling, fundamentally advancing both basic research and clinical diagnostics.

Challenges in AI-microfluidic integration

While AI-enhanced microfluidic platforms serve as powerful tools for fundamental research, biotechnological development, and clinical diagnostics, their broader adoption is hindered by several interconnected challenges. A critical appraisal reveals a significant gap between theoretical promises and practical performance. The throughput and accuracy of these systems are often overestimated; real-world performance with complex patient samples frequently fails to meet theoretical speeds, creating bottlenecks for real-time diagnostics.[25] This is because many systems are fine-tuned for ideal conditions rather than optimized for the inherent variability of clinical specimens. Accuracy in multi-parametric analysis remains compromised by inherent trade-offs; impedance-based methods are vulnerable to cell position-induced signal errors, while mechanical characterization suffers from sample variability.[25,161]

Furthermore, the scalability of these systems is constrained by material limitations and complex fabrication processes. PDMS, widely used for its biocompatibility and optical properties, exhibits batch-to-batch variability and long-term degradation.[162] The selection of AI models involves significant trade-off, sand there is a tendency to overestimate their capabilities while underestimating their limitations. CNNs provide high accuracy for image-based classification

but require large, labeled datasets and are computationally intensive.[163] Recurrent neural networks (RNNs), including long short-term memory (LSTM) networks, effectively process time-series data but face challenges with vanishing gradients and require extensive training.[164] The interpretability of models like SVM comes at the cost of performance on high-dimensional data, while the hybrid architectures like CNN-LSTM increase model complexity, often demanding specialized hardware.[165–167] The operational complexity and cost of sophisticated microfluidic chips, combined with the computational resources required for AI-driven data analysis, present further barriers to widespread clinical adoption.

Finally, the integration of AI, while promising, relies on extensive annotated datasets that are scarce for many biological scenarios.[25] The "black-box" nature of deep learning models also limits interpretability, hindering their acceptance in clinical decision-making.[168–170] Addressing these limitations requires a concerted focus on optimizing real-world performance, improving raw data acquisition, developing robust and scalable fabrication methods, and creating explainable AI models that integrate domain-specific knowledge.

Future microfluidic systems are anticipated to operate with full automation, delivering user-friendly outputs suitable for clinical settings. The evolution of data standardization and protocol automation will enhance the consistency and reliability of assays. Multifunctional integration within microfluidic chips—combining cell separation, culture, and analysis modules—will improve experimental efficiency and throughput. The extensive application of AI and machine learning algorithms will enable real-time parameter adjustments, process optimization, and result analysis, reducing human error and increasing accuracy.

Summary

This review summarizes various single-cell mechanical property characterization techniques for assessment of parameters such as cell rigidity and viscoelasticity. The methods discussed include perforated extrusion, pipette aspiration, and deformation induced by shear and stretch forces. Although these methods have yielded promising laboratory results, their clinical applicability remains limited. Conventional microfluidic chips often suffer from high sample heterogeneity, cell aggregation, and separation challenges, compromising measurement accuracy and throughput, thereby hindering clinical testing that demands high sensitivity and large-scale data acquisition. In contrast, the integration of external physical fields with AI emerges as a transformative solution, with AI serving as the core driver of advancement. External physical fields—such as acoustic pressure distributions, high-resolution optical imaging, precise electric field manipulation, and magnetic microrobots for cell capture—enable fast, convenient, and high-throughput single-cell manipulation. However, it is the integration of AI that truly unlocks their transformative potential. This goes beyond accelerating analysis to address fundamental challenges intractable for conventional methods. It enhances the entire experimental pipeline, from perception (automated cell tracking) and analysis (real-time parameter extraction) to control (adaptive feedback). More profoundly, it enables the decoding of cellular mechanical heterogeneity and predictive mechanophenotyping by learning direct mappings from complex data to intrinsic properties. However, challenges remain in data standardization, model interpretability, and system scalability. Overcoming these barriers will be essential to realize the full potential of intelligent microfluidic systems in revolutionizing mechanobiology research, point-of-care diagnostics, and personalized medicine.

Conflicts of interest

There are no conflicts to declare.

Data availability

No primary research results, software or code have been included and no new data were generated or analysed as part of this review.

Acknowledgements

This research was supported in part by the National Natural Science Foundation of China under Grant 62273052 and W2431050, the Beijing Natural Science Foundation under Grant L248102 and IS23062, and in part by the Grant-in-Aid for Scientific Research under Grant 23K22712 from the Ministry of Education, Culture, Sports, Science and Technology of Japan.

Notes and references

1 Y. Hao, S. Cheng, Y. Tanaka, Y. Hosokawa, Y. Yalikun and M. Li, *Biotechnol. Adv.*, 2020, **45**, 107648.
2 N. Bonakdar, R. Gerum, M. Kuhn, M. Spörrer, A. Lippert, W. Schneider, K. E. Aifantis and B. Fabry, *Nat. Mater.*, 2016, **15**, 1090–1094.
3 A. C. De Luca, G. Rusciano, R. Ciancia, V. Martinelli, G. Pesce, B. Rotoli, L. Selvaggi and A. Sasso, *Opt. Express*, 2008, **16**(11), 7943–7957.
4 S. Golfier, P. L. Rosendahl, A. Mietke, M. Herbig, J. R. Guck and O. Otto, *Cytoskeleton*, 2017, **74**, 283–296.
5 X. Wang, H. Liu, M. Zhu, C. Cao, Z. Xu, Y. Tsatskis, K. Lau, C. Kuok, T. Filleter, H. McNeill, C. A. Simmons, S. Hopyan and Y. Sun, *J. Cell Sci.*, 2018, **131**, jcs209627.
6 A. C. Hodgson, C. M. Verstreken, C. L. Fisher, U. F. Keyser, S. Pagliara and K. J. Chalut, *Lab Chip*, 2017, **17**(5), 805–813.
7 M. A. Bickel, D. M. Sherry, E. C. Bullen, M. L. Vance, K. L. Jones, E. W. Howard and S. M. Conley, *Microvasc. Res.*, 2024, **151**, 104609.
8 L. M. Al-Hashimi, L. Gambling and H. J. McArdle, *J. Membr. Biol.*, 2015, **248**, 1199–1206.

9 A. Mirzaaghaian, A. Ramiar, A. A. Ranjbar and M. E. Warkiani, *J. Biomech.*, 2020, **112**, 110066.
10 S. Byun, S. Son, D. Amodei, N. Cermak, J. Shaw, J. H. Kang, V. C. Hecht, M. M. Winslow, T. Jacks, P. Mallick and S. R. Manalis, *Proc. Natl. Acad. Sci. U. S. A.*, 2013, **110**, 7580–7585.
11 F. J. Armistead, J. Gala De Pablo, H. Gadêlha, S. A. Peyman and S. D. Evans, *Sci. Rep.*, 2020, **10**, 3254.
12 M. U. Hashmi and S. R. Abbas, in *Single-Cell Omics*, ed. D. Barh and V. Azevedo, Academic Press, 2019, pp. 197–220, DOI: 10.1016/B978-0-12-817532-3.00013-X.
13 N. Toepfner, C. Herold, O. Otto, P. Rosendahl, A. Jacobi, M. Kräter, J. Stächele, L. Menschner, M. Herbig, L. Ciuffreda, L. Ranford-Cartwright, M. Grzybek, Ü. Coskun, E. Reithuber, G. Garriss, P. Mellroth, B. Henriques-Normark, N. Tregay, M. Suttorp, M. Bornhäuser, E. R. Chilvers, R. Berner and J. Guck, *eLife*, 2018, **7**, e29213.
14 O. Otto, P. Rosendahl, A. Mietke, S. Golfier, C. Herold, D. Klaue, S. Girardo, S. Pagliara, A. Ekpenyong, A. Jacobi, M. Wobus, N. Töpfner, U. F. Keyser, J. Mansfeld, E. Fischer-Friedrich and J. Guck, *Nat. Methods*, 2015, **12**, 199–202.
15 J. R. Staunton, B. L. Doss, S. Lindsay and R. Ros, *Sci. Rep.*, 2016, **6**, 19686.
16 B. J. Briscoe, K. S. Sebastian and M. J. Adams, *J. Phys. D: Appl. Phys.*, 1994, **27**, 1156.
17 S. Ahmadi, P. Sukprasert, R. Vegesna, S. Sinha, F. Schischlik, N. Artzi, S. Khuller, A. A. Schäffer and E. Ruppin, *Nat. Commun.*, 2022, **13**, 1613.
18 C. G. Fonseca, V. Silvério, D. Barata, W. Giese, H. Gerhardt, S. Cardoso and C. A. Franco, *Microsyst. Nanoeng.*, 2023, **9**, 114.
19 Y. Zheng, J. Nguyen, Y. Wei and Y. Sun, *Lab Chip*, 2013, **13**, 2464–2483.
20 M. Urbanska, H. E. Muñoz, J. Shaw Bagnall, O. Otto, S. R. Manalis, D. Di Carlo and J. Guck, *Nat. Methods*, 2020, **17**, 587–593.
21 Y. Qiang, J. Liu and E. Du, *Acta Biomater.*, 2017, **57**, 352–362.
22 P. Polimeno, A. Magazzù, M. A. Iatì, F. Patti, R. Saija, C. D. Esposti Boschi, M. G. Donato, P. G. Gucciardi, P. H. Jones, G. Volpe and O. M. Maragò, *J. Quant. Spectrosc. Radiat. Transfer*, 2018, **218**, 131–150.
23 X. Tang, X. Liu, P. Li, D. Liu, M. Kojima, Q. Huang and T. Arai, *IEEE Robot. Autom. Lett.*, 2021, **6**, 2978–2984.
24 A. Nguyen, M. Brandt, T. M. Muenker and T. Betz, *Lab Chip*, 2021, **21**, 1929–1947.
25 M. Taha, A. M. Pappa, H. Saleh and A. Alazzam, *Biotechnol. Rep.*, 2025, **47**, e00905.
26 S. Khakshour, M. P. Labrecque, H. Esmaeilsabzali, F. J. S. Lee, M. E. Cox, E. J. Park and T. V. Beischlag, *Sci. Rep.*, 2017, **7**, 7833.
27 Y. Tomizawa, D. F. Daggett, G. Zheng and K. Hoshino, *J. Biophotonics*, 2023, **16**, e202200238.
28 A. Link and T. Franke, *Lab Chip*, 2020, **20**, 1991–1998.
29 V. K. Yannakula, A. A. Alluri, D. Samuel, S. A. Popoola, B. A. Barake, A. Alabbasi, A. S. Ahmed, D. A. Cortes Bandy and N. J. Jesi, *Cureus*, 2025, **17**, e83464.
30 C. S. Bang, H. Lim, H. M. Jeong and S. H. Hwang, *J. Med. Internet Res.*, 2021, **23**, e25167.
31 S. Zhou, B. Chen, E. S. Fu and H. Yan, *Microsyst. Nanoeng.*, 2023, **9**, 116.
32 C. Combs, D. D. Seith, M. J. Bovyn, S. P. Gross, X. Xie and Z. S. Siwy, *Biomicrofluidics*, 2022, **16**, 014104.
33 Y. Deng, S. P. Davis, F. Yang, K. S. Paulsen, M. Kumar, R. Sinnott DeVaux, X. Wang, D. S. Conklin, A. Oberai, J. I. Herschkowitz and A. J. Chung, *Small*, 2017, **13**, 1700705.
34 M. Horade, C.-H. D. Tsai, H. Ito and M. Kaneko, *Micromachines*, 2017, **8**, 100.
35 L. Liu, M. Bi, Y. Wang, J. Liu, X. Jiang, Z. Xu and X. Zhang, *Nanoscale*, 2021, **13**, 19352–19366.
36 Z. Wang, Y. Liu, W. Lu, Y. V. Fu and Z. Zhou, *Biomed. Opt. Express*, 2021, **12**, 7568–7581.
37 A. Mustafa, D. Haider, A. Barua, M. Tanyeri, A. Erten and O. Yalcin, *Sens. Diagn.*, 2023, **2**, 1509–1520.
38 C. A. Ferguson, J. C. M. Hwang, Y. Zhang and X. Cheng, *Sensors*, 2023, **23**, 1001.
39 S. Zhang, Z. Han, H. Qi, S. Liu, B. Liu, C. Sun, Z. Feng, M. Sun and X. Duan, *Anal. Chem.*, 2024, **96**, 4419–4429.
40 X. Wang, C. Ho, Y. Tsatskis, J. Law, Z. Zhang, M. Zhu, C. Dai, F. Wang, M. Tan, S. Hopyan, H. McNeill and Y. Sun, *Sci. Robot.*, 2019, **4**, eaav6180.
41 P. Mukherjee, C. A. Patino, N. Pathak, V. Lemaitre and H. D. Espinosa, *Small*, 2022, **18**, 2107795.
42 B. Chai, C. Efstathiou, H. Yue and V. M. Draviam, *Trends Cell Biol.*, 2024, **34**, 955–967.
43 K. J. Waller, H. Saihi, W. Li, J. H. Brindley, A. De Jong, W. K. Syn, C. Bessant and W. Alazawi, *Clin. Mol. Hepatol.*, 2023, **29**, 417–432.
44 C. A. Rickert and O. Lieleg, *Biophys. Rev.*, 2022, **3**, 021306.
45 V. B. Mathema, P. Sen, S. Lamichhane, M. Oresic and S. Khoomrung, *Comput. Struct. Biotechnol. J.*, 2023, **21**, 1372–1382.
46 S. V. Stassen, G. G. K. Yip, K. K. Y. Wong, J. W. K. Ho and K. K. Tsia, *Nat. Commun.*, 2021, **12**, 5528.
47 A. Raj, M. Dixit, M. Doble and A. K. Sen, *Lab Chip*, 2017, **17**(21), 3704–3716.
48 Y. Wu, T. Cheng, Q. Chen, B. Gao, A. G. Stewart and P. V. S. Lee, *Biomicrofluidics*, 2020, **14**, 014114.
49 M. Mokbel, D. Mokbel, A. Mietke, N. Träber, S. Girardo, O. Otto, J. Guck and S. Aland, *ACS Biomater. Sci. Eng.*, 2017, **3**, 2962–2973.
50 F. J. Armistead, J. Gala De Pablo, H. Gadêlha, S. A. Peyman and S. D. Evans, *Biophys. J.*, 2019, **116**, 1127–1135.
51 D. Nguyen, L. Tao, H. Ye and Y. Li, *Mech. Mater.*, 2023, **180**, 104631.
52 M. Liang, D. Yang, Y. Zhou, P. Li, J. Zhong and Y. Ai, *Anal. Chem.*, 2021, **93**, 4567–4575.
53 M. Liang, J. Zhong and Y. Ai, *Adv. Healthcare Mater.*, 2022, **11**, e2200628.
54 H. A. Cognart, J.-L. Viovy and C. Villard, *Sci. Rep.*, 2020, **10**, 6386.
55 F. Xing, S. Xun, Y. Zhu, F. Hu, I. Drevenšek-Olenik, X. Zhang, L. Pan and J. Xu, *Biochem. Biophys. Res. Commun.*, 2019, **512**, 303–309.

56 H. Babahosseini, J. S. Strobl and M. Agah, *Anal. Methods*, 2017, **9**, 847–855.
57 X. Yang, Z. Chen, J. Miao, L. Cui and W. Guan, *Biosens. Bioelectron.*, 2017, **98**, 408–414.
58 L. Chen, K. X. Wang and P. S. Doyle, *Soft Matter*, 2017, **13**, 1920–1928.
59 Y. Zhou, D. Yang, Y. Zhou, B. L. Khoo, J. Han and Y. Ai, *Anal. Chem.*, 2018, **90**, 912–919.
60 S. Hu and R. H. W. Lam, *Microfluid. Nanofluid.*, 2017, **21**, 68.
61 T. Ye, H. Shi, N. Phan-Thien, C. T. Lim and Y. Li, *J. Biomech.*, 2019, **84**, 103–112.
62 P. Li, X. Liu, M. Kojima, Q. Huang and T. Arai, *Langmuir*, 2021, **37**, 8083–8094.
63 Z. Zhou, C. Ni, Z. Zhu, Y. Chen, Z. Ni and N. Xiang, *Lab Chip*, 2023, **23**, 4528–4539.
64 E. Ibarboure, M. Fauquignon and J.-F. Le Meins, *J. Visualized Exp.*, 2020, e60199.
65 L. de Plater, J. Firmin and J.-L. Maître, *Biophys. J.*, 2025, **124**, 901–912.
66 R. C. Boot, A. Roscani, L. van Buren, S. Maity, G. H. Koenderink and P. E. Boukany, *Lab Chip*, 2023, **23**, 1768–1778.
67 Q. Wei, Y. Xiong, Y. Ma, D. Liu, Y. Lu, S. Zhang, X. Wang, H. Huang, Y. Liu, M. Dao and X. Gong, *Lab Chip*, 2024, **24**, 305–316.
68 J. Stuart and G. B. Nash, *Blood Rev.*, 1990, **4**, 141–147.
69 K. Matthews, E. S. Lamoureux, M.-E. Myrand-Lapierre, S. P. Duffy and H. Ma, *Lab Chip*, 2022, **22**, 1254–1274.
70 C. Bosmans, N. Ginés Rodriguez, M. Karperien, J. Malda, L. Moreira Teixeira, R. Levato and J. Leijten, *Trends Biotechnol.*, 2024, **42**, 739–759.
71 K. Jain, A. Pandey, H. Wang, T. Chung, A. Nemati, P. Kanchanawong, M. P. Sheetz, H. Cai and R. Changede, *Adv. Mater.*, 2024, **36**, 2309284.
72 M. Ermis, E. Antmen and V. Hasirci, *Bioact. Mater.*, 2018, **3**, 355–369.
73 A. T. Nguyen, S. R. Sathe and E. K. F. Yim, *J. Phys.: Condens. Matter*, 2016, **28**, 183001.
74 M. Gupta, L. Kocgozlu, B. R. Sarangi, F. Margadant, M. Ashraf and B. Ladoux, in *Methods in Cell Biology*, ed. E. K. Paluch, Academic Press, 2015, vol. 125, pp. 289–308.
75 P. De Saram, N.-T. Nguyen, S. Jamali and N. Kashaninejad, *Small Sci.*, 2025, **5**, 2400410.
76 X. He, L. Jin, Y. Qin, J. Zhong, Z. H. I. Ouyang and Y. E. Zeng, *Biocell*, 2024, **48**, 1521–1529.
77 A. Khadpekar, N. Dwivedi, P. Tandaiya and A. Majumder, *Cell Rep. Phys. Sci.*, 2025, **6**, 102456.
78 C. R. Pfeifer, Y. Xia, K. Zhu, D. Liu, J. Irianto, V. M. M. García, L. M. S. Millán, B. Niese, S. Harding, D. Deviri, R. A. Greenberg and D. E. Discher, *Mol. Biol. Cell*, 2018, **29**, 1948–1962.
79 X. Li, B. Fan, L. Liu, D. Chen, S. Cao, D. Men, J. Wang and J. Chen, *Sci. Rep.*, 2018, **8**, 14229.
80 Y. Li, Y. Li, C. Liu, X. Yu, Z. Gan, L. Xiang, J. Zheng, B. Meng, R. Yu, X. Chen, X. Kou, Y. Cao and T. Ai, *Stem Cells Transl. Med.*, 2024, **13**, 812–825.
81 K. Deshmukh, S. Gupta, K. Mitra and A. Bit, *Micromachines*, 2022, **13**, 1766.
82 R. H. Pires, N. Shree, E. Manu, E. Guzniczak and O. Otto, *Philos. Trans. R. Soc., B*, 2019, **374**, 20190081.
83 Q. Xiao, Y. He, M. H. Rahman, G. Cheng, R. Zhou and Y.-P. Ho, *View*, 2023, **4**, 20220049.
84 P. Rosendahl, K. Plak, A. Jacobi, M. Kraeter, N. Toepfner, O. Otto, C. Herold, M. Winzi, M. Herbig, Y. Ge, S. Girardo, K. Wagner, B. Baum and J. Guck, *Nat. Methods*, 2018, **15**, 355–358.
85 Y. Zheng, M. A. Cachia, J. Ge, Z. Xu, C. Wang and Y. Sun, *Lab Chip*, 2015, **15**, 3138–3146.
86 B. Fregin, F. Czerwinski, D. Biedenweg, S. Girardo, S. Gross, K. Aurich and O. Otto, *Nat. Commun.*, 2019, **10**, 415.
87 Y. Liu, K. Zografos, J. Fidalgo, C. Duchêne, C. Quintard, T. Darnige, V. Filipe, S. Huille, O. du Roure, M. S. N. Oliveira and A. Lindner, *Soft Matter*, 2020, **16**, 9844–9856.
88 K. Zografos, F. Pimenta, M. A. Alves and M. S. Oliveira, *Biomicrofluidics*, 2016, **10**, 043508.
89 M. Masaeli, D. Gupta, S. O'Byrne, H. T. K. Tse, D. R. Gossett, P. Tseng, A. S. Utada, H.-J. Jung, S. Young, A. T. Clark and D. Di Carlo, *Sci. Rep.*, 2016, **6**, 37863.
90 Y. Chen, C. Ni, L. Jiang, Z. Ni and N. Xiang, *Small*, 2024, **20**, 2303962.
91 L. Guillou, J. B. Dahl, J.-m. G. Lin, A. I. Barakat, J. Husson, S. J. Muller and S. Kumar, *Biophys. J.*, 2016, **111**(9), 2039–2050.
92 D. R. Gossett, H. T. K. Tse, S. A. Lee, Y. Ying, A. G. Lindgren, O. O. Yang, J. Rao, A. T. Clark and D. Di Carlo, *Proc. Natl. Acad. Sci. U. S. A.*, 2012, **109**, 7630–7635.
93 J. S. Dudani, D. R. Gossett, H. T. K. Tse and D. Di Carlo, *Lab Chip*, 2013, **13**, 3728–3734.
94 H. T. K. Tse, D. R. Gossett, Y. S. Moon, M. Masaeli, M. Sohsman, Y. Ying, K. Mislick, R. P. Adams, J. Rao and D. Di Carlo, *Sci. Transl. Med.*, 2013, **5**, 212ra163.
95 J. Lin, D. Kim, H. T. Tse, P. Tseng, L. Peng, M. Dhar, S. Karumbayaram and D. Di Carlo, *Microsyst. Nanoeng.*, 2017, **3**, 17013.
96 L. M. Lee and A. P. Liu, *Lab Chip*, 2015, **15**, 264–273.
97 D. Dannhauser, M. I. Maremonti, V. Panzetta, D. Rossi, P. A. Netti and F. Causa, *Lab Chip*, 2020, **20**, 4611–4622.
98 S. J. Hymel, H. Lan and D. B. Khismatullin, *Biophys. J.*, 2020, **119**, 493–501.
99 F. Wei, K. Flowerdew, M. Kinzel, L. E. Perotti, J. Asiatico, M. Omer, C. Hovell, V. Reumers and M. J. Coathup, *Bone Res.*, 2022, **10**, 65.
100 T. H. Song, M. Cao, J. Min, H. Im, H. Lee and K. Lee, *APL Bioeng.*, 2025, **9**, 036107.
101 E. Du, M. Dao and S. Suresh, *Extreme Mech. Lett.*, 2014, **1**, 35–41.
102 Y. Teng, K. Zhu, C. Xiong and J. Huang, *Anal. Chem.*, 2018, **90**(14), 8370–8378.
103 R. Lownes Urbano and A. Morss Clyne, *Lab Chip*, 2016, **16**, 561–573.
104 Y. Qiang, J. Liu, M. Dao, S. Suresh and E. Du, *Proc. Natl. Acad. Sci. U. S. A.*, 2019, **116**, 19828–19834.

105 O. A. Penuela, F. Palomino and L. A. Gómez, *Rev. Bras. Hematol. Hemoter.*, 2016, **38**, 15–20.
106 E. O. Adekanmbi and S. K. Srivastava, *Lab Chip*, 2016, **16**, 2148–2167.
107 S. Hu, T. Liu, C. Xue, Y. Li, Y. Yang, X. Xu, B. Liu, X. Chen, Y. Zhao and K. Qin, *Anal. Methods*, 2022, **14**, 4813–4821.
108 Y. Feng, J. Zhu, H. Chai, W. He, L. Huang and W. Wang, *Small*, 2023, **19**, 2303416.
109 B. Zhu, Y. Cai, Z. Wu, F. Niu and H. Yang, *IEEE Access*, 2019, **7**, 152224–152232.
110 H. Yang, M. Zhu, T. Chen, F. Niu, L. Sun and L. Cheng, *iScience*, 2022, **25**, 104275.
111 Y. Feng, Z. Cheng, H. Chai, W. He, L. Huang and W. Wang, *Lab Chip*, 2022, **22**, 240–249.
112 F. Merola, Á. Barroso, L. Miccio, P. Memmolo, M. Mugnano, P. Ferraro and C. Denz, *Cytometry, Part A*, 2017, **91**, 527–533.
113 W. G. Lee, H. Bang, H. Yun, J. Lee, J. Park, J. K. Kim, S. Chung, K. Cho, C. Chung, D.-C. Han and J. K. Chang, *Lab Chip*, 2007, **7**, 516–519.
114 K. B. Roth, K. B. Neeves, J. Squier and D. W. M. Marr, *Cytometry, Part A*, 2015, **89**, 391–397.
115 G. Trotta, R. Martínez Vázquez, A. Volpe, F. Modica, A. Ancona, I. Fassi and R. Osellame, *Micromachines*, 2018, **9**, 388.
116 C. T. Mierke, *Front. Cell Dev. Biol.*, 2019, **7**, 184.
117 Z. Yao, C. C. Kwan and A. W. Poon, *Lab Chip*, 2020, **20**, 601–613.
118 T. Sawetzki, C. D. Eggleton, S. A. Desai and D. W. M. Marr, *Biophys. J.*, 2013, **105**, 2281–2288.
119 M. S. Yousafzai, F. Ndoye, G. Coceano, J. Niemela, S. Bonin, G. Scoles and D. Cojoc, *Opt. Lasers Eng.*, 2016, **76**, 27–33.
120 Y. Liu, Z. Wang, Z. Zhou and T. Xiong, *Spectrochim. Acta, Part A*, 2022, **277**, 121274.
121 W. Hardiman, M. Clark, C. Friel, A. Huett, F. Perez-Cota, K. Setchfield, A. J. Wright and M. Tassieri, *Acta Biomater.*, 2023, **166**, 317–325.
122 J. F. Berret, *Nat. Commun.*, 2016, **7**, 10134.
123 M. Monticelli, D. V. Conca, E. Albisetti, A. Torti, P. P. Sharma, G. Kidiyoor, S. Barozzi, D. Parazzoli, P. Ciarletta, M. Lupi, D. Petti and R. Bertacco, *Lab Chip*, 2016, **16**, 2882–2890.
124 C. Garzon-Coral, H. A. Fantana and J. Howard, *Science*, 2016, **352**, 1124–1127.
125 D. Hartono, Y. Liu, P. L. Tan, X. Y. S. Then, L.-Y. L. Yung and K.-M. Lim, *Lab Chip*, 2011, **11**, 4072–4080.
126 P. Augustsson, J. T. Karlsen, H.-W. Su, H. Bruus and J. Voldman, *Nat. Commun.*, 2016, 7.
127 S. Deshmukh, Z. Brzozka, T. Laurell and P. Augustsson, *Lab Chip*, 2014, **14**, 3394–3400.
128 Y. Wu, A. G. Stewart and P. V. S. Lee, *Lab Chip*, 2021, **21**, 2812–2824.
129 H. G. Lim, O. J. Lee, K. K. Shung, J.-T. Kim and H. H. Kim, *Cancers*, 2020, **12**, 1212.
130 T. A. Allen, *Cancers*, 2024, **16**, 1377.
131 Y. Xie, N. Nama, P. Li, Z. Mao, P. H. Huang, C. Zhao, F. Costanzo and T. J. Huang, *Small*, 2016, **12**, 902–910.
132 S. J. Raymond, D. J. Collins, R. O'Rorke, M. Tayebi, Y. Ai and J. Williams, *Sci. Rep.*, 2020, **10**, 8745.
133 X. Guo, M. Sun, Y. Yang, H. Xu, J. Liu, S. He, Y. Wang, L. Xu, W. Pang and X. Duan, *Adv. Sci.*, 2021, **8**, 2002489.
134 M. Rezayati Charan, F. Berg and P. Augustsson, *Phys. Rev. Appl.*, 2023, **19**, 014046.
135 P. M. Graybill, R. Bollineni, Z. Sheng, R. V. Davalos and R. Mirzaeifar, *Biomicrofluidics*, 2021, **15**(2), 024103.
136 A. Saadat, D. A. Huyke, D. I. Oyarzun, P. V. Escobar, I. H. Øvreeide, E. S. G. Shaqfeh and J. G. Santiago, *Lab Chip*, 2020, **20**, 2927–2936.
137 K. G. Birmingham, I. E. Robinson, E. E. Edwards and S. N. Thomas, *Lab Chip*, 2020, **20**, 806–822.
138 Y. Man, D. H. Wu, R. An, P. Wei, K. Monchamp, U. Goreke, Z. Sekyonda, W. J. Wulftange, C. Federici, A. Bode, L. V. Nayak, J. A. Little and U. A. Gurkan, *Sens. Diagn.*, 2023, **2**, 457–467.
139 Y. Wu and Y. Meng, *TrAC, Trends Anal. Chem.*, 2023, **168**, 117301.
140 Y. Qiang, J. Liu, M. Dao and E. Du, *Lab Chip*, 2021, **21**, 3458–3470.
141 J.-C. Chien, A. Ameri, E.-C. Yeh, A. N. Killilea, M. Anwar and A. M. Niknejad, *Lab Chip*, 2018, **18**, 2065–2076.
142 H. A. Phan, A. N. Thi, N. P. Dang, H. Vu-Dinh, B. L. Dang, T. T. Bui, C.-P. Jen, L. D. Quang, H. H. Nguyen and T. C. Duc, presented in part at the *2023 1st International Conference on Health Science and Technology (ICHST)*, 2023.
143 H. Wang, Z. Liu, D. M. Shin, Z. G. Chen, Y. Cho, Y.-J. Kim and A. Han, *Lab Chip*, 2019, **19**, 387–393.
144 J. Y. Hwang, J. Kim, J. M. Park, C. Lee, H. Jung, J. Lee and K. K. Shung, *Sci. Rep.*, 2016, **6**, 27238.
145 T. Yang, F. Bragheri, G. Nava, I. Chiodi, C. Mondello, R. Osellame, K. Berg-Sørensen, I. Cristiani and P. Minzioni, *Sci. Rep.*, 2016, **6**, 23946.
146 L. Huang, F. Liang, Y. Feng, P. Zhao and W. Wang, *Microsyst. Nanoeng.*, 2020, **6**, 57.
147 X. Du, D. Chang, S. Kaneko, H. Maruyama, H. Sugiura, M. Tsujii, N. Uozumi and F. Arai, *Engineering*, 2023, **24**, 94–101.
148 K. Ito, S. Sakuma, M. Kimura, T. Takebe, M. Kaneko and F. Arai, *Micromachines*, 2016, **7**, 221.
149 Y. Zhang, Y. Zhao, D. Chen, K. Wang, Y. Wei, Y. Xu, C. Huang, J. Wang and J. Chen, *Analyst*, 2019, **144**, 1008–1015.
150 E. S. Lamoureux, E. Islamzada, M. V. J. Wiens, K. Matthews, S. P. Duffy and H. Ma, *Lab Chip*, 2022, **22**, 26–39.
151 S. Warnat, H. King, C. Forbrigger and T. Hubbard, *J. Micromech. Microeng.*, 2015, **25**, 025011.
152 B. Barazani, S. Warnat, A. Fine and T. Hubbard, *J. Micromech. Microeng.*, 2017, **27**, 025002.
153 D. Chang, S. Sakuma, K. Kera, N. Uozumi and F. Arai, *Lab Chip*, 2018, **18**, 1241–1249.
154 M. Naeem, M. Fiorino, P. Addabbo and A. Coronato, presented in part at the *Communication Papers of the 19th Conference on Computer Science and Intelligence Systems (FedCSIS)*, 2024.
155 X. Yang and J. Gao, *Comput. Mol. Biol.*, 2024, **14**, 125–133.

156 M. Gao, C. Song, Q. Zhang, X. Zhang, Y. Li and F. Yuan, *J. Imaging*, 2025, **11**, 307.
157 H. T. H. Phan, A. Kumar, D. Feng, M. Fulham and J. Kim, *IEEE Trans. Med. Imaging*, 2019, **38**, 1477–1487.
158 B. K. Chinni and C. Manlhiot, *Can. J. Cardiol.*, 2024, **40**, 1880–1896.
159 P. Zhang, P. Li, M. Tang, R. C. Gimple, L. Huang, J. Yue, Q. Shen, Y. Du, Q. Zhang, Z. Yang, H. He, K. Yang, L. Zhao and S. Zhou, *Sci. China: Life Sci.*, 2024, **67**, 1549–1562.
160 D. Nguyen, L. Tao, H. Ye and Y. Li, *Mech. Mater.*, 2023, **180**, 104631.
161 R. Oria, K. Jain and V. M. Weaver, *npj Biol. Phys. Mech.*, 2025, **2**, 9.
162 M. Taha, A. M. Pappa, H. Saleh and A. Alazzam, *Biotechnol. Rep.*, 2025, **47**, e00905.
163 S. S. Yadav and S. M. Jadhav, *J. Big Data.*, 2019, **6**, 113.
164 S. Das, A. Tariq, T. Santos, S. S. Kantareddy and I. Banerjee, in *Machine Learning for Brain Disorders*, ed. O. Colliot, Springer US, New York, NY, 2023, pp. 117–138, DOI: 10.1007/978-1-0716-3195-9_4.
165 Y. Peng and M. H. Nagata, *Chaos, Solitons Fractals*, 2020, **139**, 110055.
166 J. P. Gygi, S. H. Kleinstein and L. Guan, *Hum. Vaccines Immunother.*, 2023, **19**, 2251830.
167 W. Chen, W. Hussain, F. Cauteruccio and X. Zhang, *Comput. Model. Eng. & Sci.*, 2023, **139**, 187–224.
168 E. ŞAhiN, N. N. Arslan and D. Özdemir, *Neural Comput. Appl.*, 2025, **37**, 859–965.
169 Q. Xu, W. Xie, B. Liao, C. Hu, L. Qin, Z. Yang, H. Xiong, Y. Lyu, Y. Zhou and A. Luo, *J. Healthc. Eng.*, 2023, **2023**, 9919269.
170 K. M. Adnan, T. M. Ghazal, M. Saleem, M. S. Farooq, C. Y. Yeun, M. Ahmad and S.-W. Lee, *Sci. Rep.*, 2025, **15**, 19223.

Volume 26
Number 6
17 March 2026
Pages 1789–2102

Lab on a Chip

Devices and applications at the micro- and nanoscale

rsc.li/loc

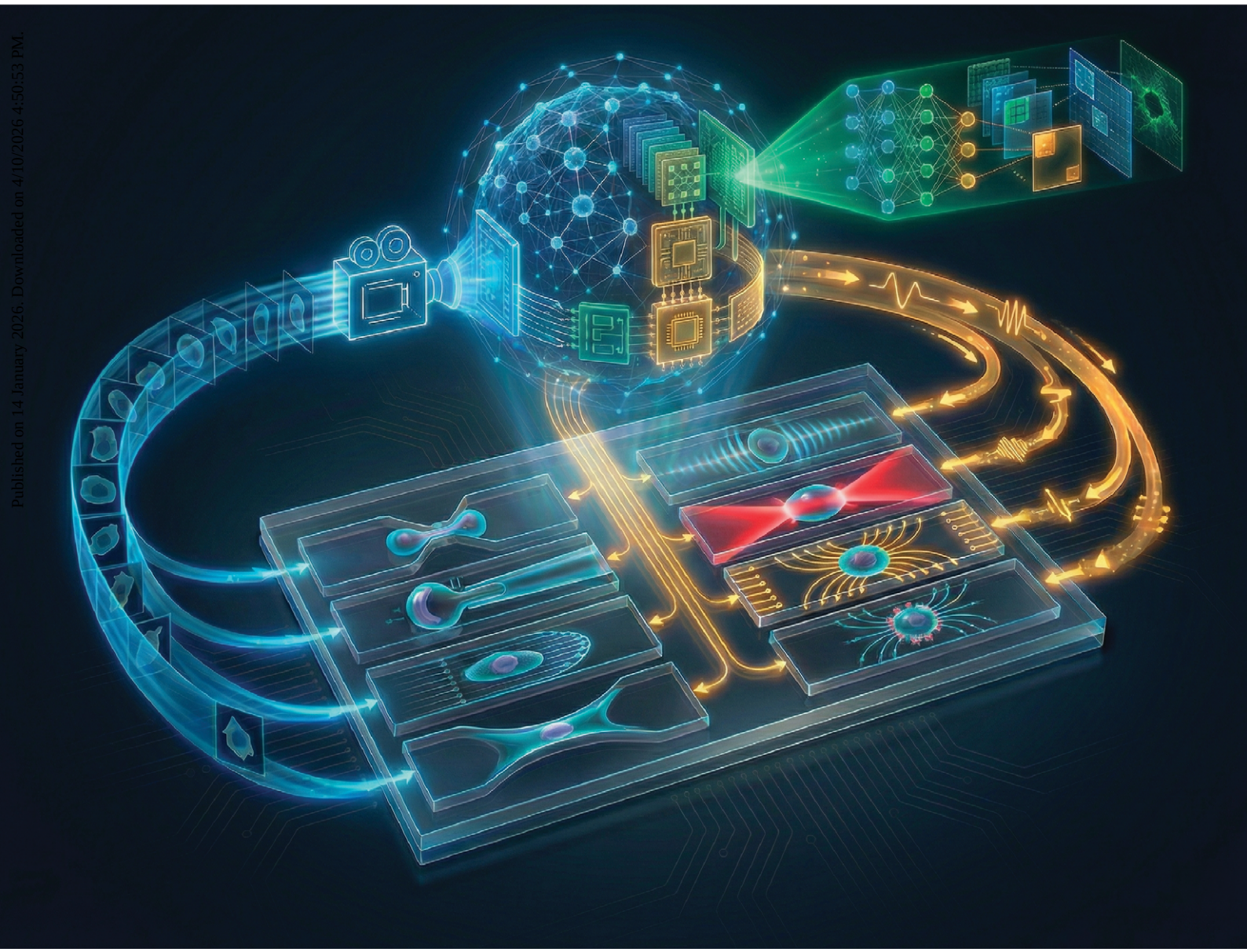

ISSN 1473-0197

ROYAL SOCIETY OF CHEMISTRY

See Xiaoming Liu, Zhuo Chen *et al.*, pp. 1528-1546.
Image reproduced by permission of Xiaoming Liu from *Lab Chip*, 2026, **26**, 1528.

25 YEARS ANNIVERSARY